

Technical University of Crete
Electronics and Computer Engineering Department



Diploma thesis

**Study of Pupil Response to Multiwavelength Excitation
In Normal and Pathologic Conditions**

Dretaki Paraskevi

Committee:

Professor Balas Costas (Supervisor)

Associate Professor Mania Aikaterini

Dr Kortsalioudakis Nathanail

October 2015

“Study of Pupil Response to Multiwavelength Excitation in Normal and Pathologic Conditions”

Abstract

Pupillography is a non-invasive method to record changes of the diameter of the pupil, in response to a given light stimulus. The pupillary reflex is controlled by the Autonomous Nervous System (ANS), thus the changes occur subconsciously. This arises the interest for further research, in order to associate pupil response with mental and brain pathologies. Throughout literature, there is lack of a compact and portable device with increased accuracy and reliability. This thesis presents a novel device for pupil examination, with various stimulants within the visible spectrum. Moreover, a simple graphical interface was developed, including the design of an acquisition interface for measurements. A custom image processing algorithm provides record of the diameter of the pupil through time. Three protocols, that ensure result credibility, were defined and a group of participants was dedicated. Measurement results provide a variety of parameters for further study and some references towards normal pupil behavior. These references map basic information essential to initiate further clinical researches. Due to the relation of the pupillary reflexes and the ANS functionality, the presented device provides a valuable and easy to use tool in a variety of applications, from research of clinical issues, to psychological impacting conditions such as sleep deprivation and alcohol intoxication.

Table of Contents

Introduction	8
Chapter1: Biological view.....	9
1.1 The eye.....	9
1.2 The pupil	10
1.2.1 Miosis.....	10
1.2.2 Mydriasis.....	10
1.3 Autonomic Nervous System.....	10
1.3.1 Physiologic Anatomy of the Sympathetic Nervous System	11
1.3.2 Physiologic Anatomy of the Parasympathetic Nervous System	12
1.4 Autonomic Nervous System Summary	13
1.5 Physiology of the photomotor reflex.....	14
1.6 Pupillary Light Reflex.....	15
Chapter 2: Pupillography till today and statement of purpose	17
2.1 Introduction in PLR.....	17
2.2 Research in pupil reflex.....	17
2.2.1 PLR and sleepiness	17
2.2.2 Drugs and alcohol.....	17
2.2.3 PLR and psychiatric disorders and anxiety.....	18
2.2.4 Brain and mental disorders.....	18
2.2.5 Eye diseases	19
2.2.6 Diabetes and Cardiovascular Neuropathy	19
2.3 PLR Devices.....	19
2.4 Statement of purpose	22
Chapter 3: Device instrumentation	22
3.1 Cameras CMOS sensors	22
3.2 Infrared LEDs.....	23
3.3 LEDs Specifications.....	24
3.3.1 White LED.....	25
3.3.2 Monochromatic LEDs.....	25
3.4 IR pass optical filters	28
3.5 Microcontroller	30
3.5 LED Driver IC.....	30
3.6 LED Driving Printed Circuit Board (PCB).....	31
3.7 The device	34

Chapter 4: Acquisition method and software development	36
4.1 Algorithmic issues	36
4.2 Algorithmic accuracy.....	38
4.3 Acquisition method.....	39
4.4 Software Development	42
4.4.1 Capturing video Graphical User Interface (GUI)	42
4.4.2 Calculation Graphical User Interface (GUI).....	43
Chapter 5: Methods and Results	44
5.1 General Schedule	44
5.2 Protocols	44
5.3 Results	45
5.3.1 Pupillograms	45
5.3.2 Parameter analysis.....	48
5.3.3 A different Subject	52
5.4 Discussion and Future Work	56
References	58
Appendix	61

List of Figures and Tables

Figure 1. 1 Human Eye	9
Figure 1. 2 The cranial nerves	13
Figure 1. 3: ANS	13
Figure 1. 4: The reflex arc.....	14
Figure 1. 5: Pathways of Pupillary light reflex.....	16
Figure 2. 1: Colvard pupillometer.....	20
Figure 2. 2: Prototype model developed in our laboratory.....	20
Figure 2. 3: Eye tracking system composed of a head-mounted goggle and control box	21
Figure 2. 4: RAPDX device	21
Figure 2. 5: A prototype of the TrueField Analyzer	21
Figure 3. 1: Cmos sensor and micro lens	23
Figure 3. 2: Infrared LED.....	23
Figure 3. 3: IR LED response	24
Figure 3. 4: White LED response	25
Figure 3. 5: 740nm LED response	28
Figure 3. 6: Transmission curve of the filter.....	29
Figure 3. 7: ATmega328	30
Figure 3. 8: TLC5940.....	31
Figure 3. 9: First step, Printed Circuit Board design	33
Figure 3. 10: IR led placement to avoid white spots in the images by producing domed illumination	33
Figure 3. 11: First stages of development	34
Figure 3. 12: Final device.....	35
Figure 3. 13: Inside view of the device	35
Figure 4. 1: Three contour points	37
Figure 4. 2: The geometrical data from previous steps.....	37
Figure 4. 3: Pupil's algorithmic estimation.....	38
Figure 4. 4: Semi-closed eyes	38
Figure 4. 5: Diameter measured in nm and the algorithmic results in pixels.....	39
Figure 4. 6: Manage Calibration Sets GUI.....	40
Figure 4. 7: PLR test path	41
Figure 4. 8: Examinee information GUI.....	42
Figure 4. 9: Capturing GUI.....	43
Figure 4. 10: Calculation GUI	44
Figure 5. 1 : Pupil response in white led stimulus in the left eye	45
Figure 5. 2: Pupil response in white led stimulus in the right eye	46

<i>Figure 5. 3: Pupil response in white led stimulus in the left eye with various intensities</i>	46
<i>Figure 5. 4: Pupil response in white led stimulus in the right eye with various intensities</i>	47
<i>Figure 5. 5: Pupil response with stimulus in the left eye</i>	47
<i>Figure 5. 6: Pupil response with stimulus in the right eye</i>	48
<i>Figure 5. 7: Parameters definition diagram</i>	49
<i>Figure 5. 8: Expected behavior in different intensities</i>	50
<i>Figure 5. 9: Experimental behavior in different intensities</i>	51
<i>Figure 5. 10: Theoretical and experiment behavior in different wavelengths</i>	51
<i>Figure 5. 11: Stimulus in the left eye in 430nm- First measurement</i>	52
<i>Figure 5. 12: Stimulus in the left eye in 430nm- Second measurement</i>	52
<i>Figure 5. 13: Stimulus in the left eye in 515nm- First measurement</i>	53
<i>Figure 5. 14: Stimulus in the right eye in 515nm- First measurement</i>	53
<i>Figure 5. 15: Stimulus in the left eye in 515nm- Second measurement</i>	53
<i>Figure 5. 16: Stimulus in the right eye in 515nm- Second measurement</i>	54
<i>Figure 5. 17: Stimulus in the left eye in 587nm- First measurement</i>	54
<i>Figure 5. 18: Stimulus in the right eye in 587nm- First measurement</i>	54
<i>Figure 5. 19: Stimulus in the left eye in 587nm- Second measurement</i>	55
<i>Figure 5. 20: Stimulus in the right eye in 587nm- Second measurement</i>	55
<i>Figure 5. 21: Stimulus in the left eye in 644nm- First measurement</i>	55
<i>Figure 5. 22: Stimulus in the left eye in 644nm- Second measurement</i>	56
<i>Table 1: ANS Summary Table</i>	14
<i>Table 3. 1: Long pass filter specifications</i>	29
<i>Table 4. 1Median value and standard error table</i>	39
<i>Table A. 1 Parameter D1</i>	61
<i>Table A. 2 Parameter D2</i>	61
<i>Table A. 3 Parameter CR%</i>	62
<i>Table A. 4 Parameter PR%</i>	62
<i>Table A. 5 Parameter t1</i>	63
<i>Table A. 6 Parameter t2</i>	63
<i>Table A. 7 Parameter CR%/t1</i>	64
<i>Table A. 8 Parameters for the sixth subject</i>	65

Introduction

Pupillary light reflex is a real time window for the autonomous nervous system functionality with an uprising research interest in various clinical studies. Despite the popularity, it remains underestimated. It is used mostly to check the reflex's existence (direct and indirect) and the speed, using subjective criteria. This study introduces a new custom pupillography device and presents three different experimental protocols and their results. The goal of this thesis is to provide a reliable and complete measurement system and some references in normal subjects in order to continue the study in clinical subjects.

In Chapter 1, biological background is shortly described. Basic physiology knowledge for the human vision and the human eye, autonomous nervous system and pupillary light reflex is provided.

Chapter 2 is a presentation of the different domains where the pupillography is involved and all the already existed devices.

Chapter 3 contains the instrumentation and the setup of the device and Chapter 4 the developed algorithm and the software needs of the study.

The results, the analysis of the parameters, the discussion conclusions are presented in Chapter 5.

Chapter1: Biological view

1.1 The eye

The human visual system can be regarded as consisting of two parts. The eyes act as image receptors which capture light and convert it into signals which are then transmitted to image processing centers in the brain

Eyes are the organs of vision. They detect light and convert it into electro-chemical impulses in neurons. In higher organisms, the eye is a complex optical system; it collects light from the surrounding environment; it regulates its intensity through a diaphragm; it focuses it through an adjustable assembly of lenses to form an image; it converts this image into a set of electrical signals, and it transmits these signals to the brain through complex neural pathways that connect the eye via the optic nerve to the visual cortex and other areas of the brain.

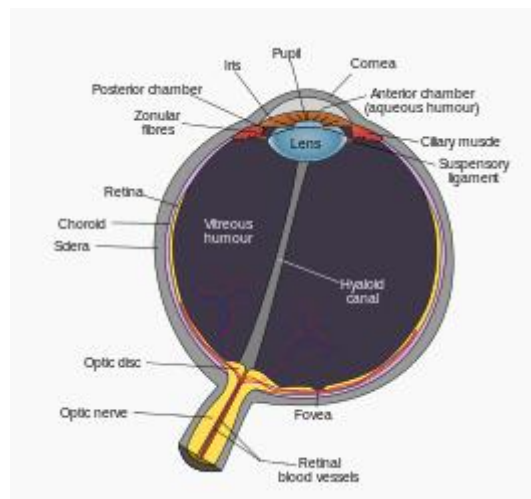


Figure 1. 1 Human Eye

The structure of the human eye is analogous to that of a camera. The basic structure of the eye is displayed in Figure 1.1

- The cornea and aqueous humour act as a primary lens which performs crude focusing of the incoming light signal.
- A muscle called the zonula controls both the shape and positioning (forward and backwards) of the eye's lens. This provides a fine control over how the light entering the eye is focused.
- The iris is a muscle which, when contracted, covers all but a small central portion of the lens. This allows dynamic control of the amount of light entering the eye, so that the eye can work well in a wide range of viewing conditions, from dim to very bright light. The portion of the lens not covered by the iris is called the pupil.

- The retina provides a photo-sensitive screen at the back of the eye, where the incoming light is focused onto. Light hitting the retina is converted into nerve signals.
- A small central region of the retina, called the fovea, is particularly sensitive because it is tightly packed with photo-sensitive cells. It provides very good resolution and is used for close inspection of objects in the visual field.
- The optic nerve transmits the signals generated by the retina to the vision processing centers of the brain.

1.2 The pupil

The pupil is a hole located in the center of the iris of the eye that allows light to strike the retina. It appears black, because light rays entering the pupil are either absorbed by the tissues inside the eye directly, or they are absorbed after diffusing reflections within the eye that mostly miss exiting the narrow pupil. In optical terms, the anatomical pupil is the eye's aperture and the iris is the aperture stop. As part of the pupillary light reflect, the pupil dilates in the dark and constricts in the light to respectively improve visibility at night and to protect the retina from sunlight damage during the day.

1.2.1 Miosis

The constriction of the human pupil is known as miosis. This is a normal reaction to a light increase. It could be also associated with certain pathological conditions, drug use or microwave radiation exposure.

1.2.2 Mydriasis

Mydriasis is the dilation of the pupil, usually defined as when having a non-physiological cause, but sometimes defined as potentially being a physiological pupillary response. Non-physiological causes of mydriasis include disease, trauma, or the use of drugs.

1.3 Autonomic Nervous System

The autonomic nervous system (ANS) is a division of the peripheral nervous system. It's a control system that acts largely unconsciously and regulates bodily functions such as the heart rate, digestion, respiratory rate, pupillary response, urination, and sexual arousal.

Within the brain, the autonomic nervous system is regulated by the hypothalamus. It consists of autonomic neurons that conduct impulses from the central nervous system (brain and/or spinal cord) to glands, smooth muscle and cardiac muscle. ANS neurons are responsible for regulating the secretions of certain glands (i.e., salivary glands) and the regulation of heart rate and peristalsis (contraction of smooth muscle in the digestive tract), among other functions.

The ANS has two branches: the sympathetic nervous system and the parasympathetic nervous system. Both of these systems have "opposite" actions where one system activates a physiological response and the other inhibits it. In general, the sympathetic is responsible for mediating energy expenditure, while the parasympathetic is responsible for energy conservation and restoration. For example, the sympathetic mediates the "fight or flight" response and the body's response to stress, pain, and cold. Thus, the parasympathetic system is responsible for stimulation of "rest-and-digest" or "feed and breed" activities that occur when the body is at rest. Both PNS and SNS are under the regulation of upper centers, particularly the anterior and posterior hypothalamus.

1.3.1 Physiologic Anatomy of the Sympathetic Nervous System

The SNS is activated in stressful or physically demanding situations and can temporarily enhance the physical performance of the body in order to better cope with the stressor. The sympathetic division of the ANS has a thoracolumbar outflow from the CNS. The preganglionic neurons of the SNS are found within the grey matter of the lateral horns of the spinal cord within the full length of the thoracic vertebrae and the cranial lumbar vertebrae. Preganglionic neurons in the SNS are relatively short. The number of vertebral segments containing SNS preganglionic neurons has a wide variation depending on the species in question; horses have 18 thoracic segments, canines have 13 and humans have 12. In most domestic species, the cranial most 4 to 6 lumbar vertebrae contain SNS segments. These preganglionic segments are located like a string of beads along either side of the spinal cord and are referred to as sympathetic chain ganglia. In most cases, the number of sympathetic ganglia exceeds the number of spinal cord vertebrae containing the preganglionic cell bodies. SNS axons exit the spinal cord via the ventral root, thus allowing the formation of the sympathetic trunk via processes called white rami communicants, which are heavily myelinated.

When entering the sympathetic trunk, there are three possibilities for the neuron. Firstly the SNS neuron could immediately synapse within the sympathetic trunk itself. Secondly it could run up or down the sympathetic trunk prior to synapsing. Or finally it could leave the sympathetic trunk without synapsing at all and instead run to collateral ganglia. Within the abdominal cavity ventral to the lumbar vertebrae there are three sympathetic ganglia called the prevertebral ganglia where this form of specialized synapsing occurs. The

prevertebral ganglia are made up of the cranial mesenteric, caudal mesenteric and coeliac. Postganglionic fibers from these ganglia distribute to abdominal and pelvic organs.

These preganglionic fibers then branch out to form synapses with postganglionic neurons, but in doing so, each preganglionic fiber actually interconnects between neighboring sympathetic chain ganglia. Therefore, presynaptic nerve fibers from one segment of the spinal cord terminate in several ganglia and therefore activity in individual ganglia may affect many areas of the body. Postganglionic neurons then extend to target organs spread throughout the body. The exception to this rule is the adrenal medulla, as this endocrine gland receives sympathetic input directly from preganglionic nerve fibers, more specifically directly from the spinal cord. In this case, the adrenal glands are effectively modified post-ganglionic sympathetic neurons that do not have axons.

1.3.2 Physiologic Anatomy of the Parasympathetic Nervous System

The PNS is only activated during rest and can be used to regulate systems during functions such as digestion. Preganglionic parasympathetic neurons have cell bodies that are located in two separate parts of the CNS, rather than running almost the full length of the CNS as the SNS does. The PNS has preganglionic neurons located in the brain stem and the sacral part of the spinal cord, and is referred to as a craniosacral outflow. Four of the cranial nerves supply parasympathetic innervation to the majority of the body's glands and internal organs; the oculomotor nerve, facial nerve, glossopharyngeal nerve and the vagus nerve. In particular the vagus nerve (tenth cranial nerve) is responsible for a major proportion of PNS innervation, although the PNS fibers located within the lateral horns of 2 or 3 sacral segments are responsible for innervation of the sex organs, urinary bladder and the rectum. Preganglionic PNS neurons are relatively long and have their cell bodies located within the cranial nerve nuclei for cranial nerves or in the lateral horn grey matter of the spinal cord for the sacral segments. PNS ganglia are located either adjacent to or within the wall of target organs and in contrast to SNS ganglia, there are no interconnections between ganglia in the PNS. Postganglionic PNS neurons are therefore very short.

It has been stated that the parasympathetic nervous system can change faster than the sympathetic nervous system. Thus, as the sympathetic starts to mediate a stress response the parasympathetic, it immediately begins to counter it. If the parasympathetic was not faster than the sympathetic, then any stress response could send the heart into tachycardia and onto ventricular fibrillation before the parasympathetic could act to prevent it. The parasympathetic, through the vagus, is the main controlling influence on respiratory activity.

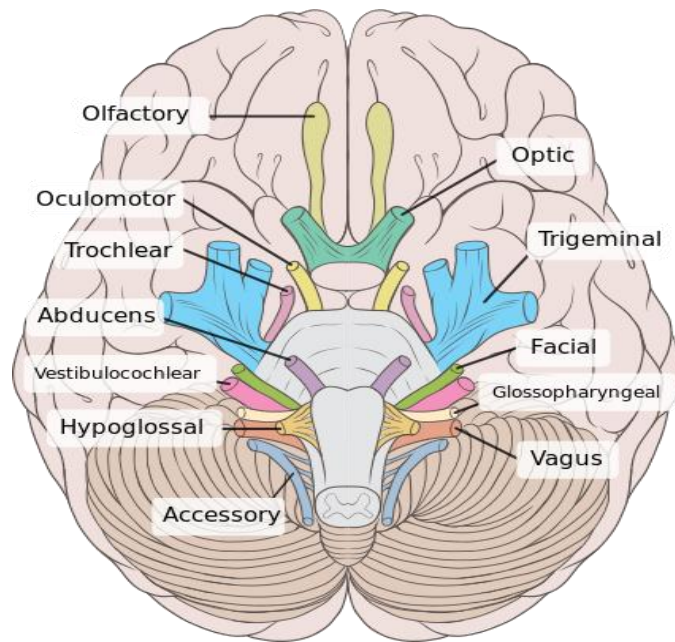


Figure 1. 2 The cranial nerves

1.4 Autonomic Nervous System Summary

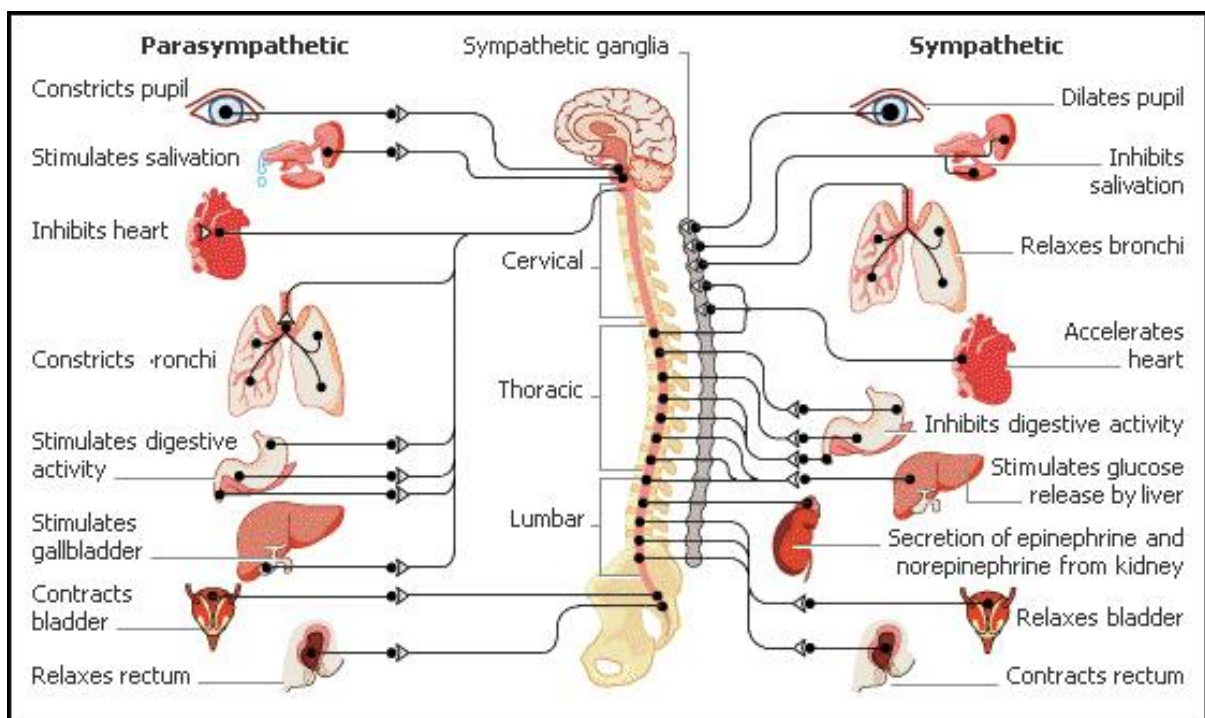


Figure 1. 3: ANS

Autonomic Nervous System

Structure	Sympathetic Stimulation	Parasympathetic Stimulation
Iris (eye muscle)	Pupil dilation	Pupil constriction
Salivary Glands	Saliva production reduced	Saliva production increased
Oral/Nasal Mucosa	Mucus production reduced	Mucus production increased
Heart	Heart rate and force increased	Heart rate and force decreased
Lung	Bronchial muscle relaxed	Bronchial muscle contracted
Stomach	Peristalsis reduced	Gastric juice secreted; motility increased
Small Intestine	Motility reduced	Digestion increased
Large Intestine	Motility reduced	Secretions and motility increased
Liver	Increased conversion of glycogen to glucose	
Kidney	Decreased urine secretion	Increased urine secretion
Adrenal medulla	Norepinephrine and epinephrine secreted	
Bladder	Wall relaxed Sphincter closed	Wall contracted Sphincter relaxed

Table 1: ANS Summary Table

1.5 Physiology of the photomotor reflex

Reflex is an automatic and unconscious change, inside or outside the human body. Every reflex follows a specific path, which consists five components (*Figure 1.4*).

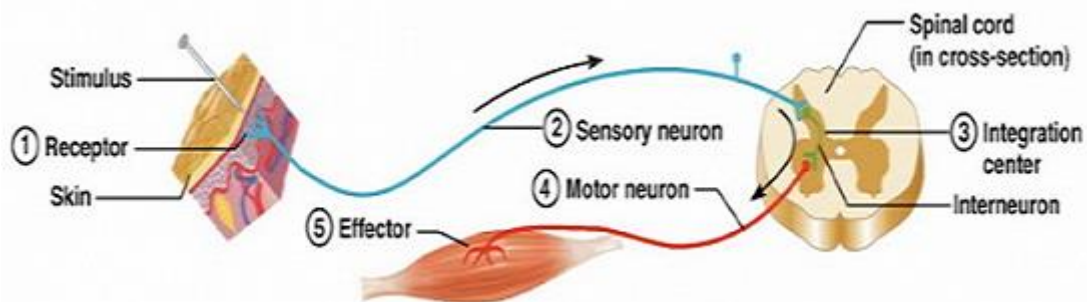


Figure 1. 4: The reflex arc

The ocular reflexes are the simplest ocular motor responses. Ocular reflexes compensate for the condition of the cornea and for changes in the visual stimulus. For example, the eye blink reflex protects the cornea from drying out and from contacting foreign objects. The pupillary light reflex compensates for changes in illumination level, whereas the accommodation responses compensate for changes in eye-to-object-viewed distance. It should be noted that reflex responses are initiated by sensory stimuli that activate afferent neurons (e.g. somatosensory stimuli for the eye blink reflex and visual stimuli for the pupillary light reflex and accommodation responses)

When the light is entering the eye, it strikes 3 different photoreceptors in retina: familiar rods, cones used in image forming, more recently discovered photosensitive ganglion cells. Ganglion cells give info ambient light levels, react sluggishly compared rods, cones. Signals photosensitive ganglion cells have multiple functions, including acute suppression of hormone melatonin, entrainment of body's circadian rhythms and regulation of size of pupil.

The retinal photoreceptors convert light stimuli electrical impulses. Nerves involved in resizing of pupil connect the pretectal nucleus of high midbrain with the bypassing lateral geniculate nucleus and the primary visual cortex. Pretectal nucleus neurons send axons neurons of edinger-westphal nucleus visceromotor axons run along both left, right oculomotor nerves. Visceromotor nerve axons (which constitute portion of cranial nerve iii, along somatomotor portion derived Edinger-Westphal nucleus) synapse on ciliary ganglion neurons, parasympathetic axons innervate iris sphincter muscle, producing miosis.

1.6 Pupillary Light Reflex

The pupillary light reflex (PLR) is a reflex that controls the diameter of the pupil, in response to the intensity (luminance) of light that falls on the retinal ganglion cells of the eye, thereby assisting in adaptation to various levels of lightness/darkness. A greater intensity of light causes the pupil to constrict (miosis-allowing less light in), whereas a lower intensity of light causes the pupil to dilate (mydriasis-allowing more light in). Thus, the pupillary light reflex regulates the intensity of light entering the eye.

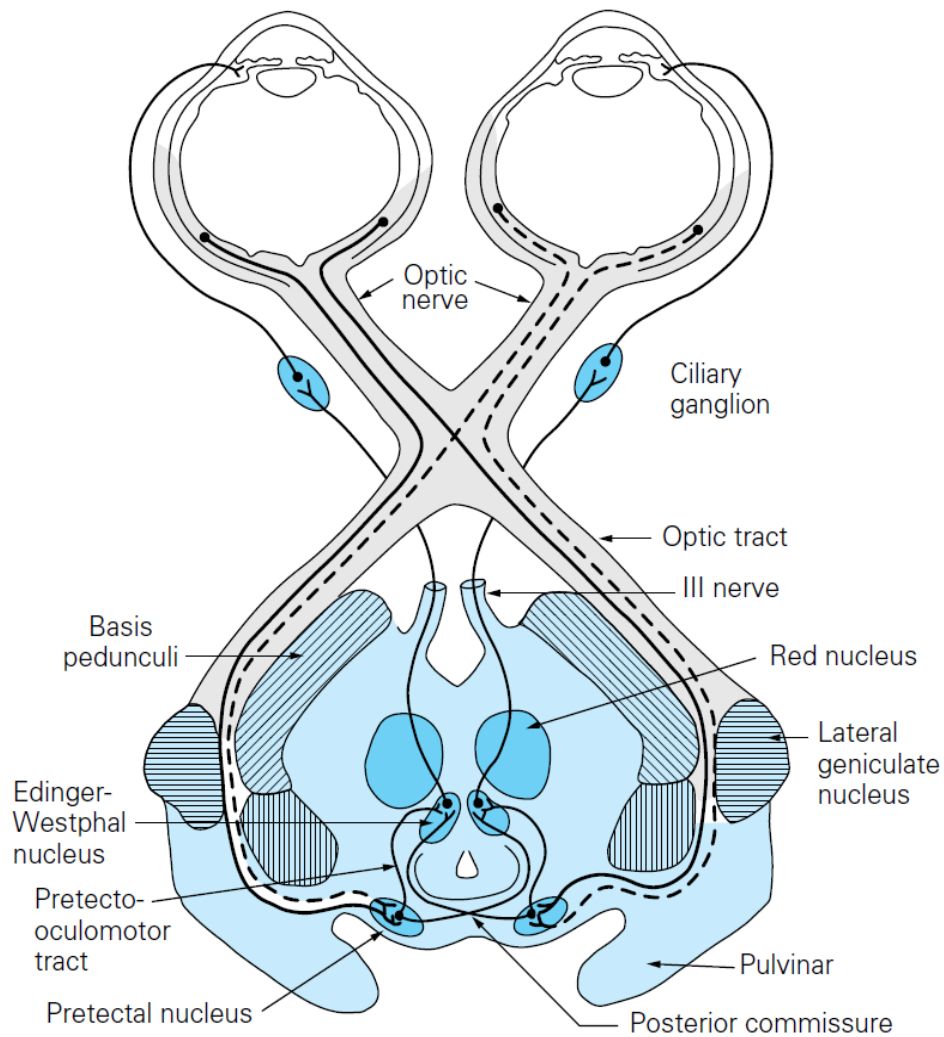


Figure 1. 5: Pathways of Pupillary light reflex

The pathway controlling pupillary light reflex involves the following:

- retina, optic nerve, optic chiasm, and the optic tract fibers that join the
- brachium of the superior colliculus, which terminate in the
- pretectal area of the midbrain, which sends most of its axons bilaterally in the posterior commissure to terminate in the
- Edinger-Westphal nucleus of the oculomotor complex, which contains parasympathetic preganglionic neurons and sends its axons in the oculomotor nerve to terminate in the
- ciliary ganglion, which sends its parasympathetic postganglionic axons in the
- short ciliary nerve, which ends on the
- iris sphincter

The pathway controlling pupil dilation involves the following:

- retina and the optic tract fibers terminating on neurons in the hypothalamus
- axons of the hypothalamic neurons that descend to the spinal cord to end on the

- sympathetic preganglionic neurons in the lateral horn of spinal cord segments T1 to T3, which send their axons out the spinal cord to end on the
- sympathetic neurons in the superior cervical ganglion, which send their
- sympathetic postganglionic axons in the long ciliary nerve to the
- iris dilator.

Chapter 2: Pupillography till today and statement of purpose

2.1 Introduction in PLR

Pupillary assessment is an important part of the neurological assessment, because changes in the size, equality and reactivity of the pupils can provide the critically ill patient with vital diagnostic information. The reaction of the pupil to light can be considered as an essential part of any clinical neurophysiological examination.

Although pupillography remains underestimated, in this chapter all the applications will be discussed and clinical surveys that consider pupillometry as a valuable diagnostic mean.

2.2 Research in pupil reflex

There is a wide variate of neuroanatomical issues where the pupil is involved. This makes the pupil an important element to be analyzed in many clinical procedures.

2.2.1 PLR and sleepiness

Besides poor sleep hygiene, shift work or psychotropic medication, sleep disorders can be caused by various neurological and psychiatric conditions. Despite the enormous importance of daytime sleepiness in sleep medicine, the available methods to assess a patient's degree of sleepiness are either time consuming or limited to the assessment of subjective feelings of sleepiness by self-rating scales. A close association between pupillometric variables and distinct changes in waking electroencephalogram (EEG) activity has been detected. The aforementioned association underscores the validity of pupillography as a time- and cost-efficient objective measure of sleepiness that could ease the diagnostic and therapeutic workup of patients, who report excessive daytime sleepiness [1]. Also, pupillographic sleepiness test (PST) in children and adolescents could be promising for the evaluation of daytime sleepiness, and should be further evaluated in future studies [2]. Another interesting pathway refers to the impact of sleep deprivation on psychophysiological reactivity to emotional stimuli [3]. The subsequent research indicates that sleep deprivation is associated with increased reactions to negative emotional information.

2.2.2 Drugs and alcohol

Drugs and alcohol are expected to affect the central nervous system and the pupil response to stimulus. PLR can function as a diagnostic mean to test the consumption of such substances. A series of findings from previous pieces of research underscore the effect of a smoked kif preparation (*Cannabis sativa* L.) on pupil diameter variations [4]. Methadone test dose pupillography provides significant information; this test is useful in diagnosing opioid dependence and is more suitable for addicts than naloxone testing [5]. A systematic review of the correlation between antidepressants and pupil reflex reveals interesting results in the field of psychopathic medicine [6]. This observation may be very useful in cases of rehabilitation from the aforementioned substances.

2.2.3 PLR and psychiatric disorders and anxiety

Pupillography could be very helpful in the science of psychiatry. There are some examples of utilization of pupillometry in psychopharmacology and mental disorders. Fear, anger or stress, dilate the pupil, an effect called the “psychosensory pupillary response”. Psychosensory pupil dilation is often less than 0.3 mm, and can be hidden within the normal, spontaneous oscillations of pupil size, which are of the same magnitude. Patients with different psychiatric disorders will display different emotional reactions to stimuli [7]. Also, anxiety is an interesting parameter to be examined and it is expected to be correlated with pupil response. Some pupilometer measurements indicate that anxiety and gender alters the pupil response to examinees [8]. Nowadays, anxiety is a common psychological issue and pupillometry is an alternative diagnostic method.

2.2.4 Brain and mental disorders

More and more people during the last decades are affected by brain and mental diseases. Early diagnosis and prediction are of vital importance for the avoidance of serious phenomena. Today, in some cases, such as Alzheimer, they can be accurately diagnosed only by histological examination of brain tissue obtained by biopsy or autopsy (post mortem). Until now, there is no early, noninvasive, sensitive and easily administered diagnostic method. Clinical studies are relating PLR and pupil sensitivity with these neurophysiological diseases. There are Pupillographic results in surveys, which correlate pupil mobility with Alzheimer disease and Parkinson’s syndrome [9], though they are still in a preliminary stage and thus they need to be further evaluated. Another survey has shown that depressed individuals were particularly slow to name the emotionality of positive information, and displayed greater sustained processing, expressed also by sustained pupil dilation [10]. Patients suffering from Schizophrenia have been studied in order to reveal the exact biophysical consequences of the disease [11]. Autism is a brain development disorder characterized by impaired social interaction, poor communication and repetitive behavior. By measuring the pupil response in children, who suffered from autism, and by comparing the results with a control group, who were not afflicted, scientists have achieved a more than 90 percent accuracy rate in separating children with autism from unaffected ones [12].

2.2.5 Eye diseases

Pupil reflex is controlled by autonomic parasympathetic nervous system and this is the reason for being theoretically connected with brain and mental diseases. There have been some research about optical issues and pupil response such as glaucoma, cataract or emmetropes and myopes patients. Pupillography experiments indicate that the odds of detecting glaucoma in the presence of asymmetric disease are increased [13] [14] [15]. Furthermore, research concerning cataract indicates the occasions, in which [16] PLR seems to be useful as additional diagnosis in certain circumstances.

2.2.6 Diabetes and Cardiovascular Neuropathy

Diabetic autonomic neuropathy involves most organs and diagnosis is largely based on cardiovascular tests. Light reflex pupillography non-invasively evaluates pupillary autonomic function [17]. Moreover, the correlations between the autonomic modulation of heart rate, blood pressure and the pupillary light reflex in healthy subjects have been examined [18]. This research reports that pupil diameter and constriction latency significantly correlated with parameters of heart rate variability, but not with those of blood pressure variability.

2.3 *PLR Devices*

There is a variety of different ways to collect a PLR dataset. The instrumentation is a significant parameter of measurements. In medicine, Colvard pupillometer is used to measure scotopic pupil size and corneal diameter of cataract and refractive candidates before surgery (Figure 2.1).



Figure 2. 1: Colvard pupillometer

Most pupil light reflex data have been collected with a tableware item. One of this model is developed in our laboratory in previous versions of the current project (Figure 2.2)

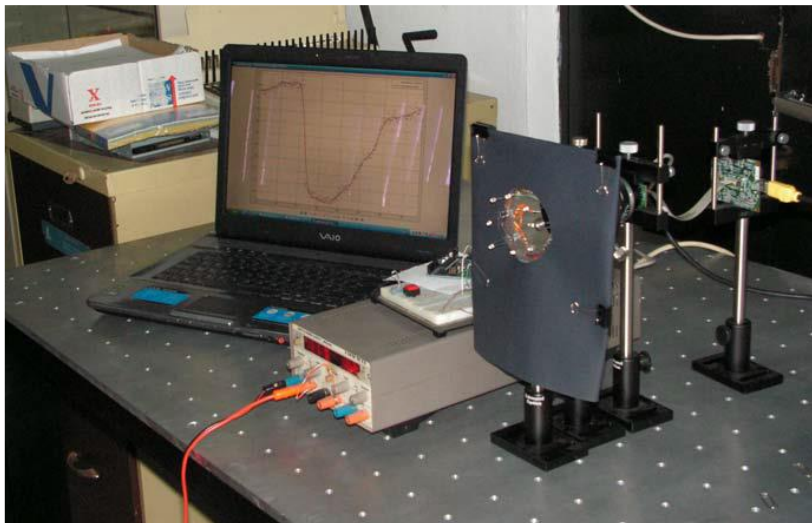


Figure 2. 2: Prototype model developed in our laboratory

Furthermore, the whole measurement system exists in a compact form such as the following one (Figure 2.3).



Figure 2. 3: Eye tracking system composed of a head-mounted goggle and control box

Apart from experimental custom devices, there are some commercial products for medicine pupillography, which are also available for the consumers. The RAPDx device is one of them (Figure 2.4) and the prototype of the TrueField Analyzer (Figure 2.5).



Figure 2. 4: RAPDX device



Figure 2. 5: A prototype of the TrueField Analyzer

2.4 Statement of purpose

In spite of the variety of devices and research, there are some details in which our project is focused on. First of all, the device or the experimental room has to provide a totally dark, quiet and relaxing environment for the measurements, so that the pupil reaction can be influenced only by the light stimulus. Secondly, our device ensures reliability due to the calibration procedure. Both eyes in different wavelengths or in a white LED stimulus have to provide the same optical effect. Moreover, most pieces of research are using white LED stimuli or red or blue or green. There is no effort to look out for information in a wide range of wavelengths. In addition, the majority of the presented devices have prohibitive size or an additional control box and as a consequence there is lack of portability and need of external power supply. The produced device is wearable and available for an operating table or an ambulance. Our custom devices fulfil all these conditions and the next chapter contains an analytic presentation of the instrumentation. Lastly, with regard to the results, the collected dataset, described in chapter 5, has the necessary characteristics to define a normalization to diameter behavior and this is a vital step before moving to clinical conditions.

Chapter 3: Device instrumentation

After studying the existed devices and describe the parameters that it is necessary to take into consideration in Chapter 2, it's time to represent the new custom and portable experimental device. The hardware components of the system are:

1. Two CMOS sensors cameras with 30fps
2. Infrared LEDs for illumination
3. White LEDs and monochromatic LEDs between 430-740nm for stimulation
4. IR pass optical filters
5. Microcontroller for synchronization

3.1 Cameras CMOS sensors

The CMOS sensor cameras are simple and very efficient, focused on the needs of our device. They offer a smooth video stream manual device properties. The chosen frame rate is 30fps and the image resolution is 640x480 pixels.



Figure 3. 1: Cmos sensor and micro lens

Specifications

- USB 2.0 fast data transfer
- Capture speed: 60 FPS
- Hardware resolution: 0.3 Mpixel
- Sensor type: 24 bit true color CMOS
- Focus: manual from 5cm to infinity
- USB cable: 1.4m
- Dimensions: 98 x 55 x 48 mm
- Net weight: 78 g

3.2 Infrared LEDs



Figure 3. 2: Infrared LED

Features

- High power Infrared LEDs

- Narrow emission angle $\pm 3^\circ$
- Very high and radiant intensity
- Short switching times
- UL version available

Characteristics

- Type SFH 4550
- Operating and storage temperature range $-40 \dots +100 \text{ }^\circ\text{C}$
- Reverse voltage V_R 5V
- Forward current I_F 100mA
- Power dissipation: 180mW
- Wavelength at peak emission 860nm
- Centroid Wavelength 850nm
- Half angle ϕ ± 3 Grad. Deg.
- Active chip area A 0.09mm^2
- Dimension of the active chip area $L \times W$: $0.3 \times 0.3 \text{ mm}^2$

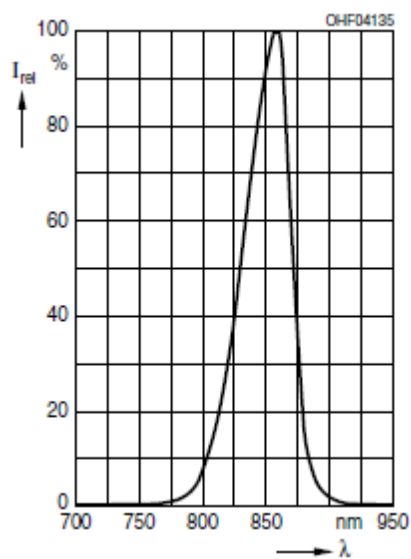


Figure 3. 3: IR LED response

3.3 LEDs Specifications

For the construction of the device twenty four leds are used. Twelve different for each eye. The one of them is a white led and the eleven others monochromatic leds.

3.3.1 White LED

This LED is a warm white simple chip Emitter LED by Nichia, model 157-AT. The package of this led is SMD. The dimensions of this LED are 3 x 1.5 x 0.5 mm. The max power dissipation of this LED is 510mW. The spectrum of the LED is illustrated bellow.

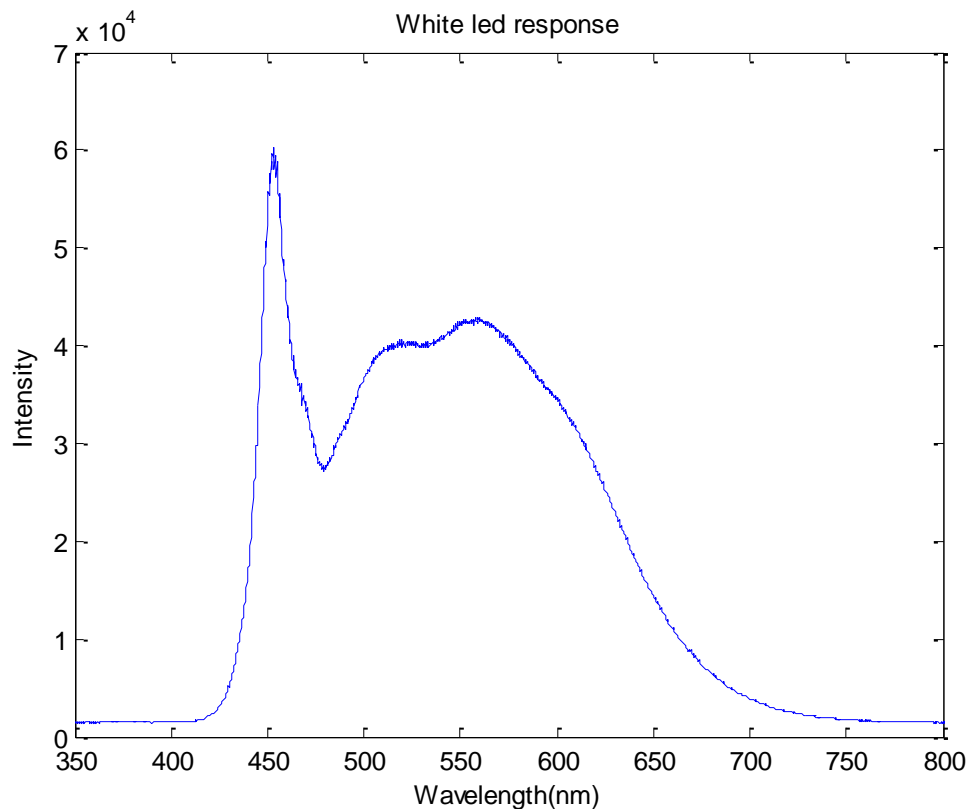


Figure 3. 4: White LED response

3.3.2 Monochromatic LEDs

In the next section, there is the presentation of the eleven monochromatic LEDs one by one and a short description of their specifications.

430 nm

This LED is a blue simple chip Emitter LED by Kingbright, model L-53MBC. The peak wavelength of this LED is $\lambda_{\text{peak}}=430\text{nm}$. It is a through hole LED with a 5mm diameter bulb. The max power dissipation of this LED is 105mW. Curve peak: 433.51nm.

458 nm

This LED is a blue simple chip Emitter LED by Forge Europa, model FNL-U300B22WCSL. The peak wavelength of this LED is $\lambda_{\text{peak}}=458\text{nm}$. It is a through hole LED with a 3mm diameter bulb. The max power dissipation of this LED is 85mW. The spectrum of the LED is illustrated bellow. Curve peak: 455.93nm.

470 nm

This LED is a blue simple chip Emitter LED by OSRAM, model LB E63C. The package of this led is SMD. The dimensions of this LED are 3.5 x 2.8 x 1.95 mm. The max power dissipation of this LED is 140mW. Curve peak: 469.61nm.

515nm

This LED is a blue-green simple chip Emitter LED by TT Electronics OPTEK Technology, model L-53MBC. The package of this LED is SMD. The dimensions of this LED are 3.5 x 2.8 x 1.95 mm. The max power dissipation of this LED is 140mW. Curve peak: 504.48nm.

535nm

This LED is a green simple chip Emitter LED by TT Electronics OPTEK Technology, model OVSAGBC2R8. The package of this LED is SMD. The dimensions of this LED are 3.5 x 2.8 x 1.95 mm. The max power dissipation of this LED is 140mW. Curve peak: 519.60nm.

569nm

This LED is a green simple chip Emitter LED by Avago Technologies, model ASMT-BB20. The peak wavelength of this LED is $\lambda_{\text{peak}}=565$. It is a through hole LED with an 8mm diameter bulb. Curve peak: 573.03nm.

587nm

This LED is a green simple chip Emitter LED by OSRAM, model LO E63B. The package of this LED is SMD. The dimensions of this LED are 3 x 3.3 x 3.8 mm. The max power dissipation of this LED is 180mW. Curve peak: 590.83nm.

605nm

This LED is an orange simple chip Emitter LED by Dialight. The package of this LED is SMD. The dimensions of this LED are 3.2 x 1.6 x 1.1 mm. The max power dissipation of this LED is 75mW. Curve peak: 614.90nm.

644nm

This LED is a hyper red simple chip Emitter LED by Kingbright, model KPTD-3216SURCK. The package of this LED is SMD. The dimensions of this LED are 3.2 x 1.6 x 1.8 mm. The max power dissipation of this LED is 75mW. Curve peak: 650.42nm.

700nm

This LED is a red simple chip Emitter LED by AND Optoelectronics, model AND123R. The peak wavelength of this LED is $\lambda_{\text{peak}}=700\text{nm}$. It is a through hole LED with a 3mm diameter bulb. The max power dissipation of this LED is 62.5mW. Curve peak: 692.62nm.

740nm

This LED is a hyper red simple chip Emitter LED by Osa Opto Light, model OIS-330 740. The package of this led is SMD. The dimensions of this led are 3.2 x 1.6 x 1.9 mm. The max power dissipation of this LED is 60mW. Curve peak: 741.50nm.

The spectrum of the LEDs is illustrated below:

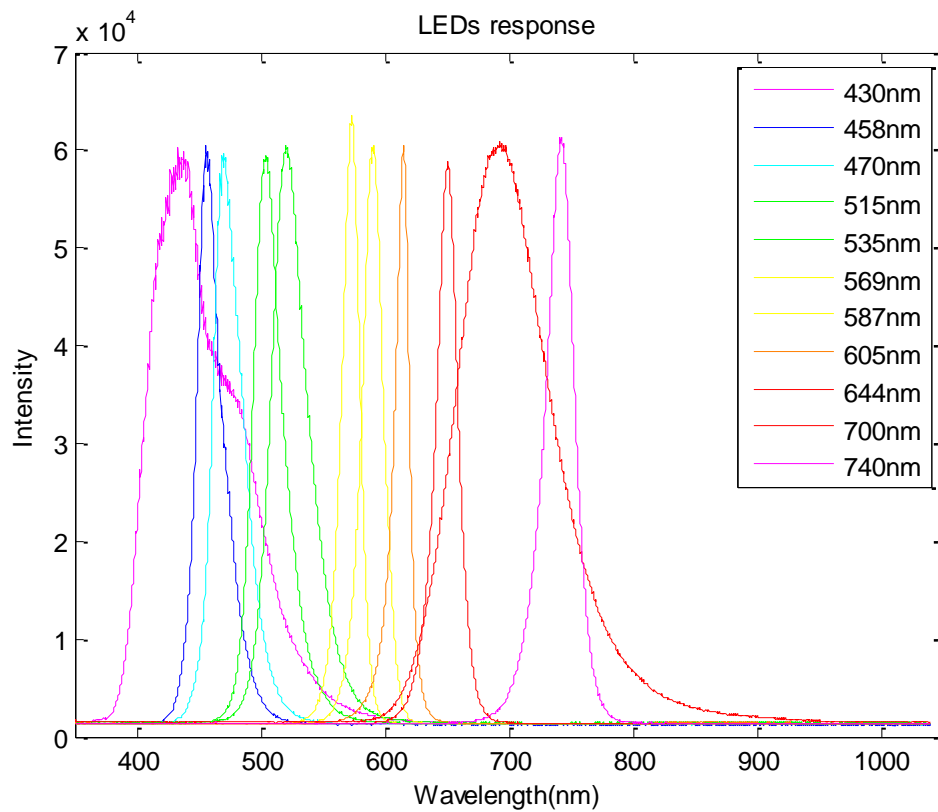


Figure 3. 5: 740nm LED response

3.4 IR pass optical filters

In order to improve the image quality, IR long-pass filters are needed. The IR long-pass filter allows only infrared light to come through and it is placed in front the lens. As a result, we have IR illumination during the executable procedure and there are no spots from the LED stimulus in images.

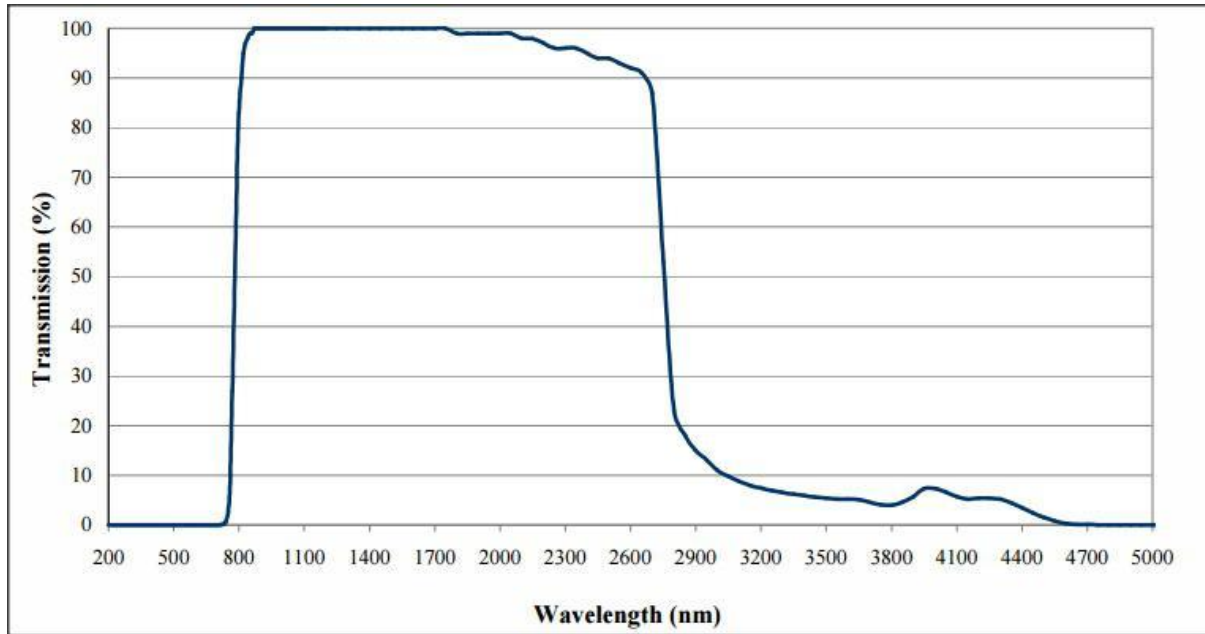


Figure 3. 6: Transmission curve of the filter

Wavelength	IR
Glass/Filter Number	Schott RG-780
Stopband Limit λ_s (nm)	610.00
Cut-Off Position λ_c (nm)	780±9
Passband Limit 1 λ_{p1} (nm)	900.00
Passband Limit 2 λ_{p2} (nm)	900.00
Spectral Transmittance t_{ip} (%)	97
Density (g/cm ³)	2.94
Transformation Temperature (°C)	552.00
Color	Black
Diameter (mm)	12.5
Dimensional Tolerance (mm)	±0.38
Thickness (mm)	3.0
Reflection Factor P_d	0.91
Surface Quality	80-50
Coating	Uncoated
Cut-On Wavelength (nm)	780
Substrate	Colored Glass
Type	Longpass Filter

Table 3. 1: Long pass filter specifications

3.5 Microcontroller

A microcontroller is needed to control and synchronize all the signals of the system. The goal is to control directly the TLC5940 LED drivers and indirectly the dimming of the LEDs, which will be presented in the next paragraph.

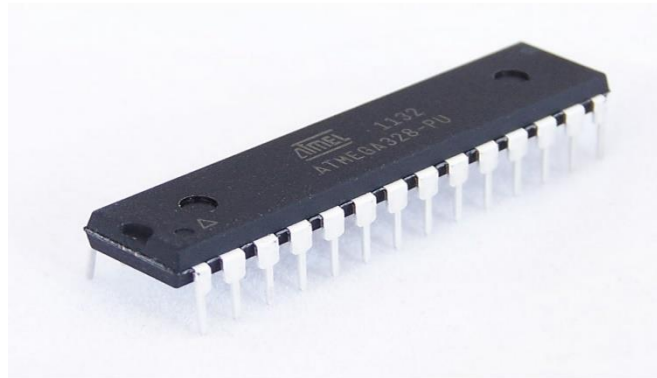


Figure 3. 7: ATmega328

The model used is the Atmel AVR ATmega328, 8-bit microcontroller, which covers the needs sufficiently. The microcontroller was mounted and preassembled on a development board. A development board also consists of complementary components to facilitate programming and incorporation into other circuits. The board includes a 5-volt linear regulator and a 16MHz crystal oscillator. The microcontroller is pre-programmed with a bootloader so that an external programmer is not necessary. The interface with the computer is done through USB connection, which is downgraded to USB-to-serial, and supportive adapter chips on the board.

3.5 LED Driver IC

The heart of the LEDs driver circuit is the TLC5940 chip by Texas Instruments. The TLC5940 is a 16-channel, constant-current sink LED driver. Each channel has an individually adjustable 4096-step grayscale PWM brightness control and a 64-step, constant-current sink (dot correction). The dot correction adjusts the brightness variations between LED channels and other LED drivers. The dot correction is stored in an integrated EEPROM. Both grayscale control and dot correction are accessible via a serial interface. A single external resistor sets the maximum current value of all 16 channels. The maximum current per channel is 130mA. Also, the maximum LED voltage is 17V.

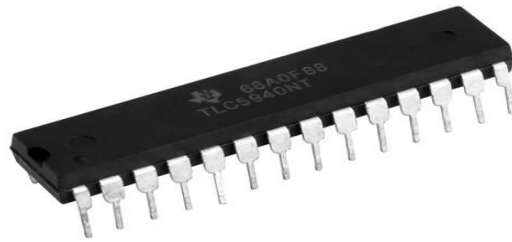


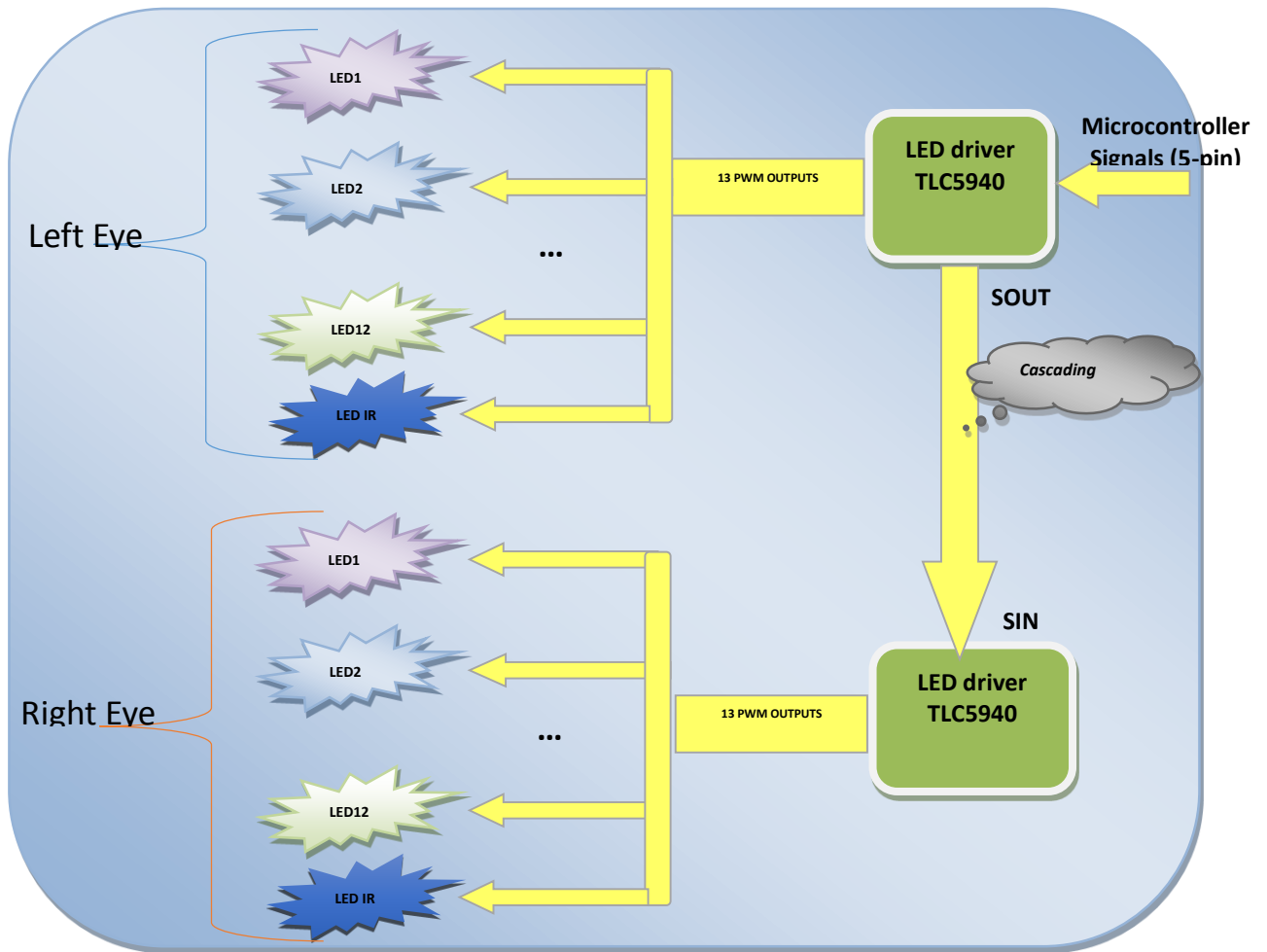
Figure 3. 8: TLC5940

3.6 LED Driving Printed Circuit Board (PCB)

After describing all the individual components of the instrumentation, it's time to present the development of the printed circuit board of the device. The process of development will be shortly presented with some images.

The heart of this device is the LED driving PCB where all LEDs, TLC5940 LED drivers, passive components and connectors are put together to consist the circuit which the microcontroller interacts with.

An abstract block diagram that describes the LED driving circuitry and design is shown below:



Microcontroller controls the TLC5940 LED drivers and each output of the TLC5940 is a PWM which adjusts the brightness of the LED.

The PCB has been designed using an electronic design automation software package. The design, which resembles as mask, is illustrated in figure 3.19. Analyzing the design, the TLC5940 LED drivers are placed diametrically opposite the ends of the board. Also, the LEDs have been placed circularly with the least diameter close to each other leaving a circular gap for the lens of the camera, as shown in the figure 3.19. In the center of the PCB there are two connectors. The small connectors is used for supplying current-voltage to the circuit. The big connector is used for communication with the microcontroller.

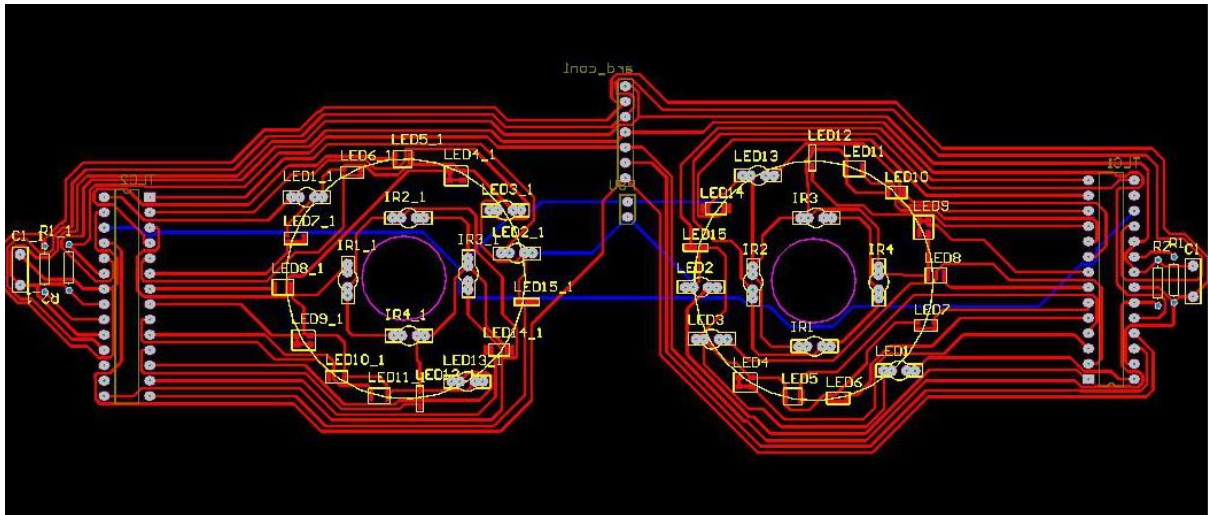


Figure 3. 9: First step, Printed Circuit Board design

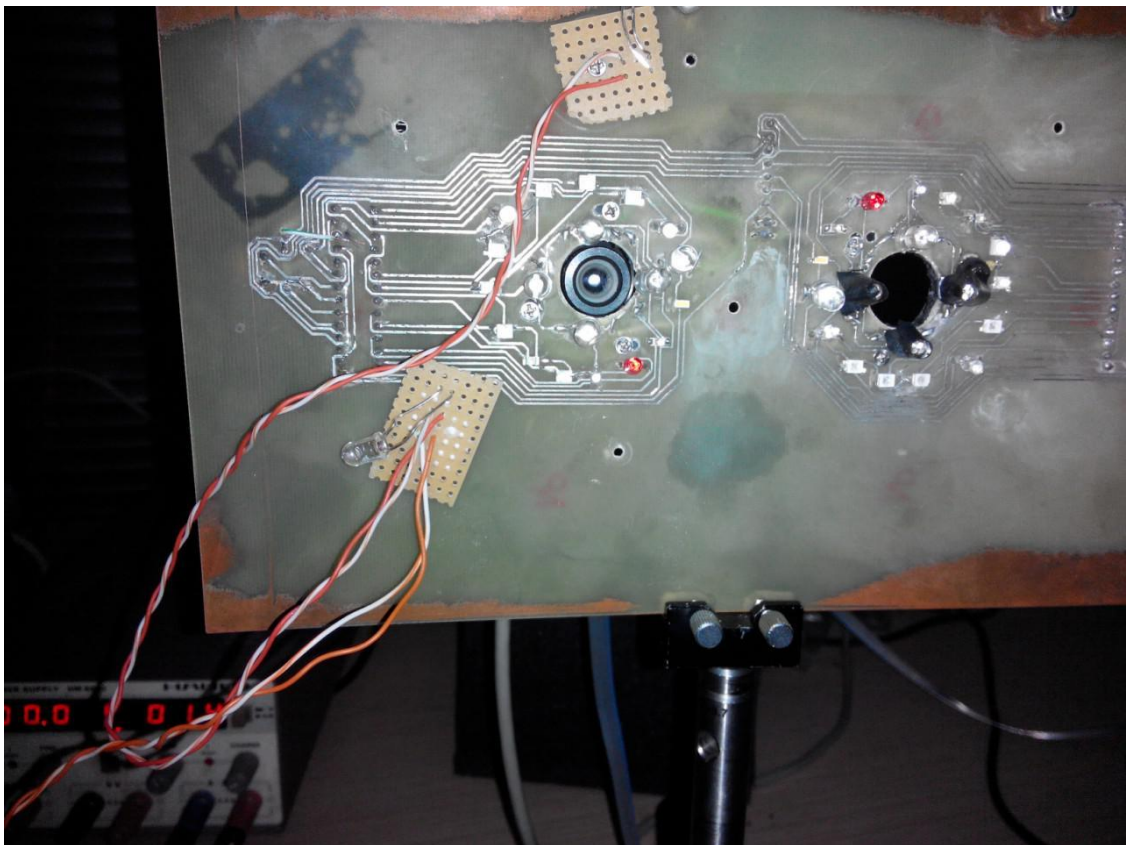


Figure 3. 10: IR led placement to avoid white spots in the images by producing domed illumination

3.7 The device

The PCB LED board which is described above has been placed on a paintball mask (with its glass removed). Holes were opened for the cameras, and the PCB and the various gaps covered with a special cloth that blocks the outside illumination.

Also a custom “jacket” has been designed for the device as a way to look beautiful and getting the correct positioning and functioning of the various components.



Figure 3. 11: First stages of development



Figure 3. 12: Final device



Figure 3. 13: Inside view of the device

Chapter 4: Acquisition method and software development

4.1 Algorithmic issues

Firstly, the purpose of this project was to develop a real time autonomous pupillography system. The idea was to obtain automatically the results in the end of the examination. So, the two main criteria of choosing the final algorithm are the execution time and the accuracy of the method.

The images are 8-bit grayscale. This means that each pixel has an intensity value between 0 – 255, where 0 is absolute black and 255 pure white. The pupil, apart from being circular is absolutely black as well. So, the pupil will be in a very black homogenous area of the image. Based on this fact, there are many complicated and time consuming algorithms for circle detection. There are also some simple algorithms based on classic geometry. The improvement in our instrumentation gave us the possibility to use a simple geometric algorithm which is based on the work of team of Cuba [18] with some changes. Below, there is a short description of this algorithm.

Step1: Crop the image

In the start of the procedure, is useful to choose correctly our region of interest (ROI). This helps us to avoid “dark pixel interference” from eyelids and eyebrows or other dark spots known as image noise.

Step2: Find an initial point inside pupil’s area

In this step, the algorithm initially searches for the maximum sequence of very dark pixels in each row and column of the picture. This process scans dark areas of the image. The threshold, below which pixels are categorized as dark, is usually under 30. In well-focused images and not over-illuminated this might be even at 0. The intersection point of these sequences will be a point in the pupil’s area. It will not be a point of something else from the face, because only the pupil has a homogenous surface of black color pixels. Also, this point will be not the center of the circle. Theoretically, it should be so, but in practice it is not, for various reasons; for instance, due to the fact that the pupil is actually not a perfect circle.

Step 3: Find 3 points in pupil’s contour

After having the initial point inside the pupil’s area, we have to define 3 points in pupil’s contour. The search of these three points begins from the point PI found in the step 1. It is known that there is a very marked texture contrast between the pupil's regions and the iris. For this reason, it is appropriate to use a quantitative texture feature, as the standard deviation, to detect the frontier between the pupil and the iris. The standard deviation feature is calculated in a point considering a vicinity of 3x3 pixels size, which is a habitual procedure in digital image analysis. The standard deviation varies slightly inside the pupil. However, it will suffer an instantaneous abrupt, increasing once the vicinity 3x3 begins to take pixels belonging to the iris region. The strategy to find the three points P1, P2 and P3 consists of the

following three trajectories with different addresses, whose angles will be 270° , 90° and 180° (Figure 1). On each point of the trajectory we compute the difference between the standard deviation of initial point P and the points of the trajectory point, whose difference is bigger than threshold, it will be selected as point belonging to the pupil's contour.

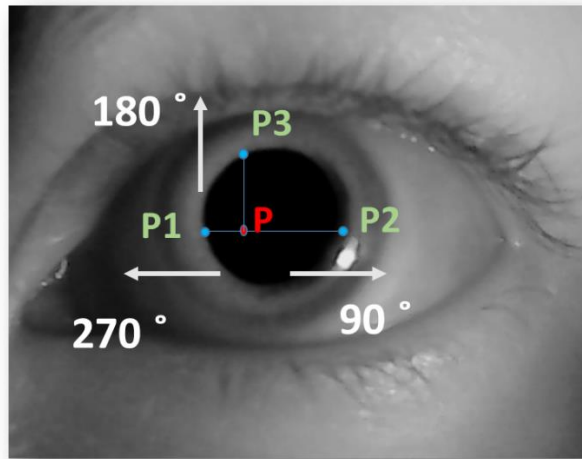


Figure 4. 1: Three contour points

Step 4: Find the pupil's diameter

Knowing the three points in the contour of the pupil is a common geometry issue to calculate the radius and the diameter.

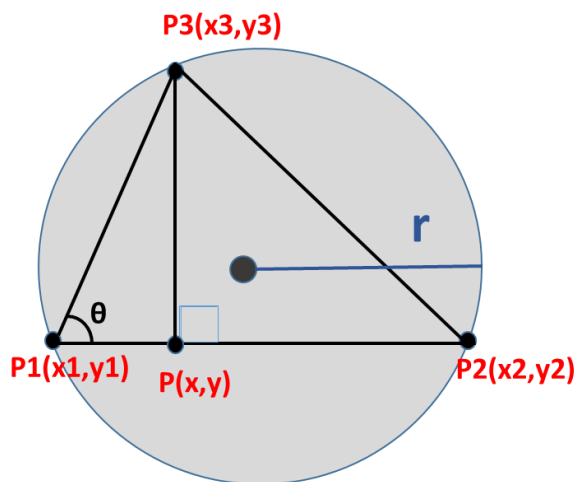


Figure 4. 2: The geometrical data from previous steps

The radius r of the circumscribed circle is calculated from the following formula:

$$r = \frac{\sqrt{(x_3-x_2)^2+(y_3-y_2)^2}}{2\sin\theta} \quad \text{and} \quad \sin\theta = \frac{\sqrt{(x_3-x)^2+(y_3-y)^2}}{\sqrt{(x_1-x_3)^2+(y_1-y_3)^2}}$$

Step 5: Draw the circle with the known diameter

To verify the accuracy and the correct algorithmic estimation, the calculated pupil is drawn in the original image.

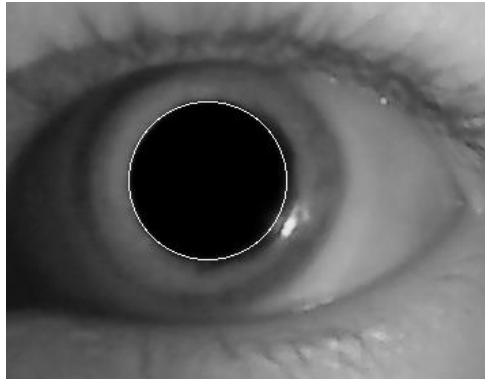


Figure 4. 3: Pupil's algorithmic estimation

Due to the perfect image quality, the efficiency of the above algorithm is significantly high. This approach has the advantage to allow the algorithm to work even when the examinee is about to start to blink or if his eye is semi-closed.

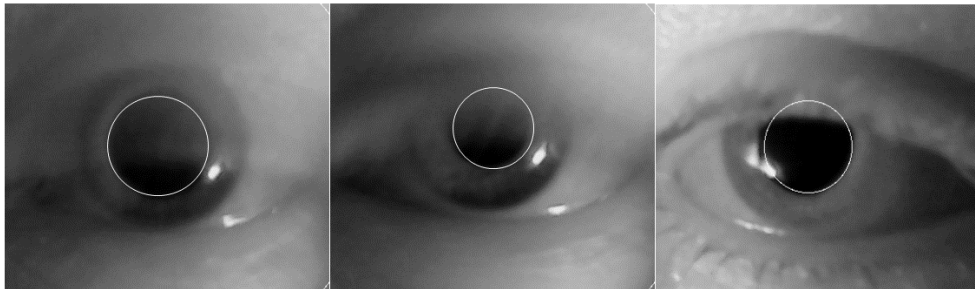


Figure 4. 4: Semi-closed eyes

4.2 Algorithmic accuracy

In order to examine the accuracy of the described algorithm, we used an artificial mutable iris with a shape really close to pupil's circle shape. So, the artificial iris was measured in mm, in seven distinct values from 2mm to 8mm. This range is defined by the real pupil's dimensions. For each distinct value of artificial iris, five different measurements have been taken. The results are gathered in the following diagram and table.

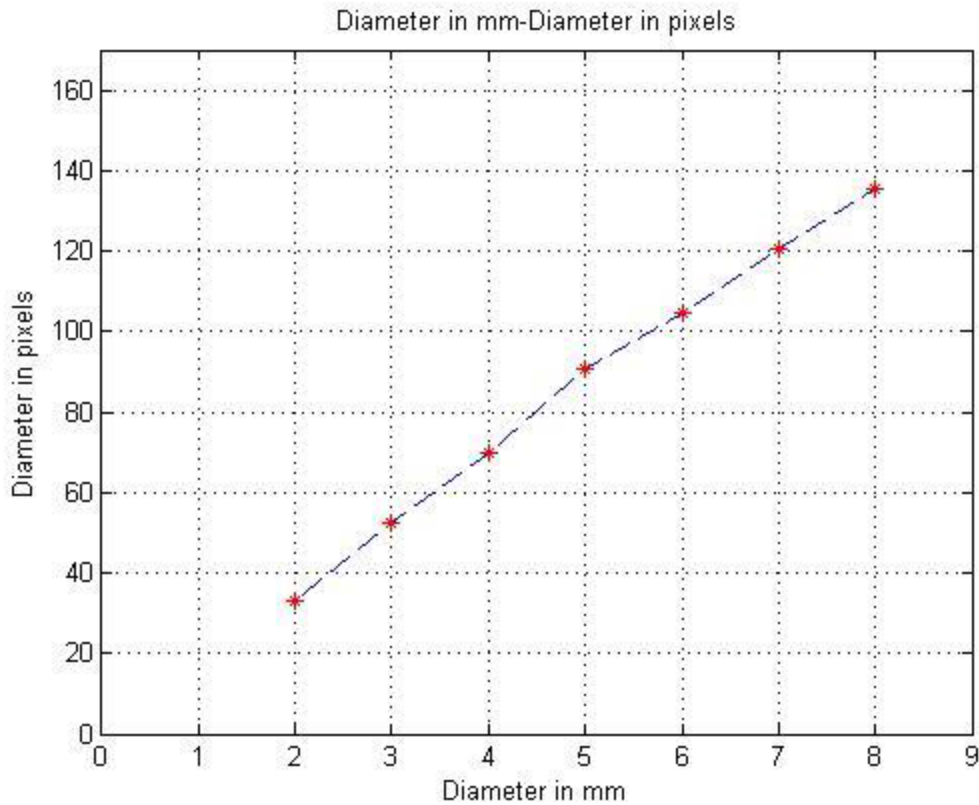


Figure 4. 5: Diameter measured in nm and the algorithmic results in pixels

Diameter in mm	2mm	3mm	4mm	5mm	6mm	7mm	8mm
MV +- SE% (pixels)	33,14+-8%	52,24+-0%	70,07+-0%	90,47+-0%	104,66+-0%	120,57+-0%	135,66+-0%

Table 4. 1Median value and standard error table

Due to previous results, it is obvious that the algorithm is reliable with almost linear behavior and zero or extremely small standard error. In 2mm the standard error value is 8% and in all the other cases this value is zero. In other words, there is a satisfying repeatability of the algorithmic procedure.

4.3 Acquisition method

The acquisition method concerns the material and the way that is used for collecting our data. The material has been described in Instrumentation chapter, so this chapter will focus on experimental procedure.

One fundamental parameter is the total time of the procedure or acquisition time. It is divided in three parts. Firstly, rest time refers to the time when the examinee stays in a dark area with no stimulus to stabilize and conform to the experimental device and procedure. Secondly, stimulation time is the time that the examinee is exposed to a specific stimulus.

This time is a short and principal parameter. In the end, recovery time completes the procedure.

The acquisition time, the IR leds optic power as the optic power and the wavelength of the stimuli is defined in Manage Calibration Sets GUI (Figure 4.2). This is the module where all the acquisition parameters are specified, except for the material parameters, which are described in previous chapter such as camera's frame rate, gain etc.

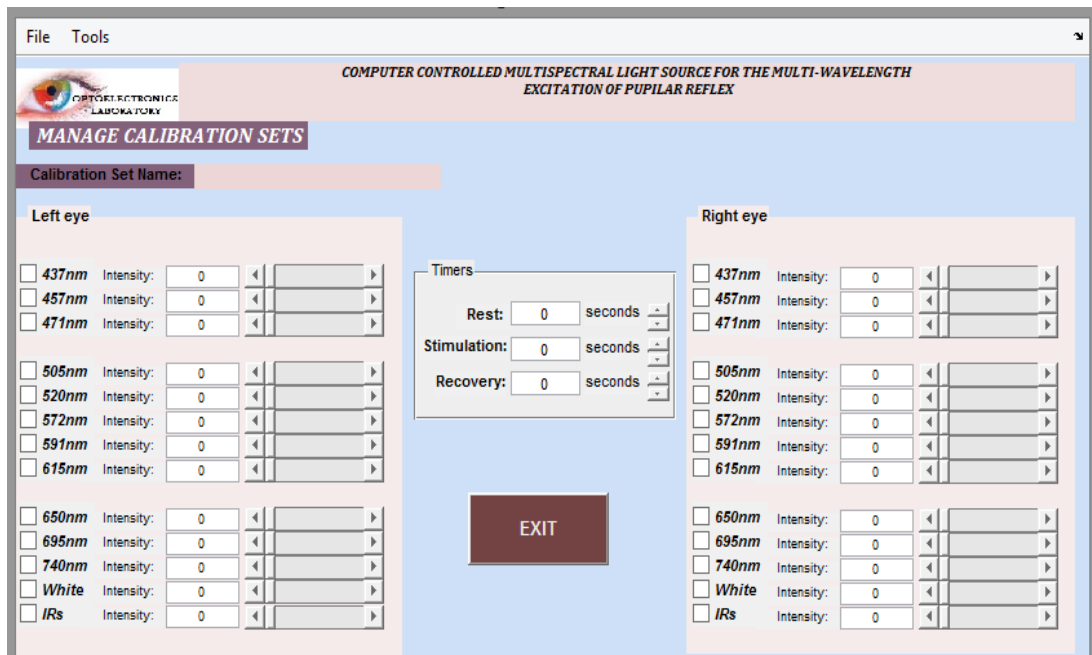


Figure 4. 6: Manage Calibration Sets GUI

Apart from the executable procedure, the whole path of measurement from the beginning until the end is displayed in the following diagram.

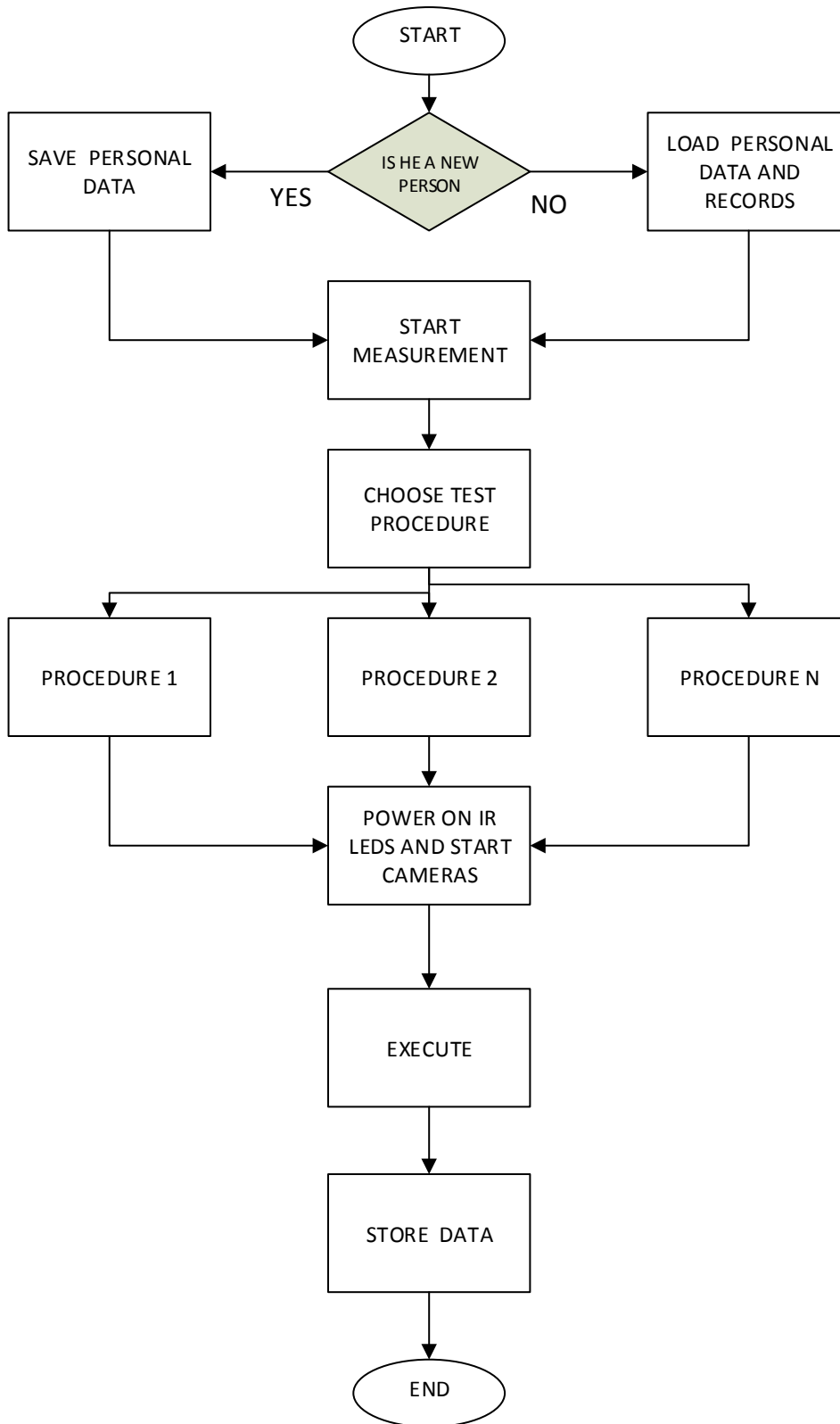


Figure 4. 7: PLR test path

The previous diagram shows shortly and effectively the experimental pathway. First of all, we have either to import a new examinee or to find an already existing from the database. Then the measurement starts, and it is time to select the desired procedure from a list of predefined tests. Subsequently, the next step is to open cameras and IR LED's and have visual contact with the examinee. After this stage, we execute the selected procedure and the data are stored in the end of execution. That's the point, when a scheduled test is completed.

4.4 Software Development

In order to make the measurement more comfortable and quick for the examinee, the procedure is divided in two stages. The first is the stage of capturing the video and the second is the stage of playing the video again and save the results.

4.4.1 Capturing video Graphical User Interface (GUI)

This stage begins with acquiring the examinee's personal information. The administrator of the test has the opportunity to add a new examinee or to load from the database an already existing examinee from a previous measurement.

The screenshot displays a graphical user interface titled "COMPUTER CONTROLLED MULTI-WAVELENGTH EXCITATION OF PUPILAR REFLEX". The interface is divided into several sections:

- Examinee Info**: A header section for the main form.
- Search/Add subject**: Contains radio buttons for "Search" and "Add".
- Demographic info**: Includes input fields for "LastName:", "FirstName:", "Date of Birth:" (with sub-fields for Day, Month, and Year), "Address:", "Postal Code:", "City:", "Home Phone:", and "Mobile Phone:". There is also a "Notes:" text area.
- Search for patient**: A search box with a "LOAD" button below it.
- Tests**: A scrollable list area for selecting tests.
- Buttons**: "SAVE" button at the bottom left, "Start Test" button at the bottom center, and "Exit" button at the bottom right.

Figure 4. 8: Examinee information GUI

After filling the form or loading an already existing examinee, the administrator presses the button 'Start Test' and the capturing video GUI opens.



Figure 4. 9: Capturing GUI

Firstly, by pressing the icon with the file in the left corner, the administrator chooses a procedure from a list of predefined procedures (in Manage Calibration Sets- Figure 4.6). The selected procedure is shown in the text box in the down section of the GUI. Secondly, by pressing the camera icon in the left corner of the window, the IR leds are opening. Lastly, by pressing the play icon, the selected procedure starts. In the end of the procedure, we have the captured video in a .mat file, which is saved in a specific file. The GUI also contains a stop button, which terminates the procedure and closes the IR leds.

4.4.2 Calculation Graphical User Interface (GUI)

After collecting the raw data, the Calculation GUI plays again the video with pupil estimation for all images and diameter calculation. First, the user has to select the file and load it by pressing the button with the file in the left corner. Then, by pressing the chosen eye button L or R, the procedure starts and the user has to select the region of interest (ROI) and to crop the image. The video is playing in the small window in the right corner and the plotted diagram in the left side shows the change of the pupil diameter in time. By using the data cursor tool (left corner) in the plotted diagram, each frame is presented in the right down corner window. This tool gives the opportunity to exclude the unfocused images or images with blinking eyes where the algorithm is possible to fail. There are also two other tools; the save button, which writes the results in an excel file and the paint button which plots the figures of the left diagram for them to be saved.

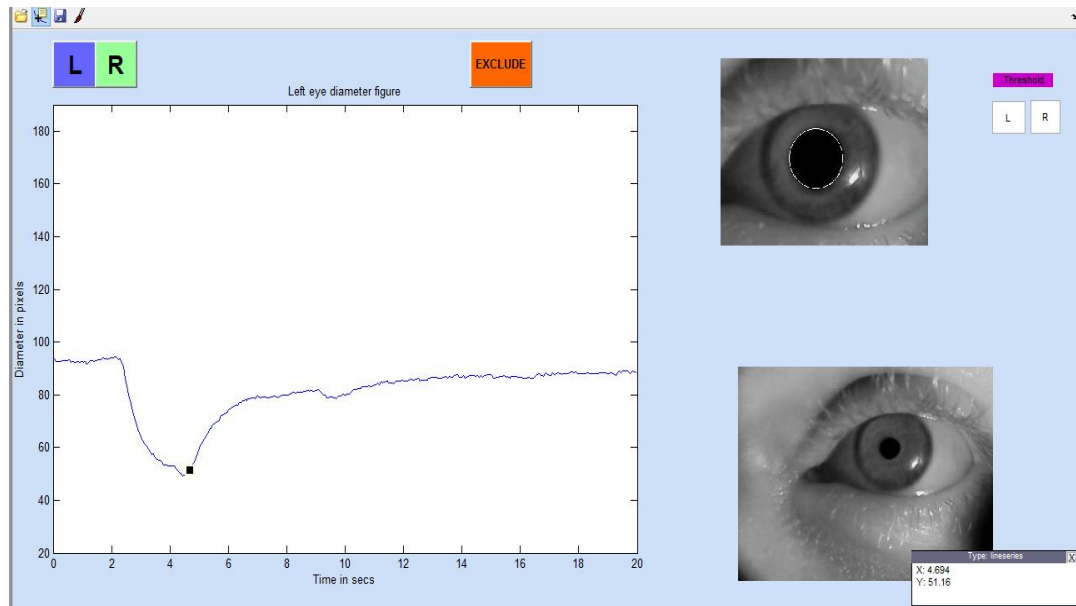


Figure 4. 10: Calculation GUI

Chapter 5: Methods and Results

5.1 General Schedule

The participants of this research are five young healthy subjects. For the recording of spontaneous pupillary behavior, the subjects were placed in a comfortable chair in a quiet room with controlled temperature between 24 to 27 °C. The experimental procedure begins when the subject wear the “measurement mask”. The whole experimental duration is divided into three parts. The first part, named as “the rest time”, refers to adaptation of the pupil in the darkness that the mask provides. In this part of the procedure, the pupil is dilated and reach the initial diameter. In “stimulation time”, the subject is exposed to the stimuli and the pupil constricts. The third part is “recovery time” when the pupil is resized to the normal dimensions. The five subjects participated in three protocols.

5.2 Protocols

The total duration of all the procedures is twenty seconds. The rest time and the stimulation time last two seconds each. Third part, the longest one, lasts sixteen seconds. In each test, both eyes are captured but only one is exposed to a stimulus. So, a completed measurement contains two twenty seconds tests, in order to cover all the combinations: left

eye with a stimulus and right eye without stimulus as left eye without stimulus and right eye with a stimulus.

Protocol 1: contains five measurements with white led stimulus with optical power of $150\mu\text{Watt}$.

Protocol 2: contains five measurements with white led stimulus with optical power from $10\mu\text{Watt}$ to $560\mu\text{Watt}$.

Protocol 3: contains measurements with eleven monochromatic led stimulus, all having the same optical power of $150\mu\text{Watt}$. The monochromatic leds wavelength range is from 430nm to 740nm.

The subjects after completing a measurement have a break of twenty to thirty minutes until the next one. Between the measurements, the consumption of food or coffee is not allowed.

5.3 Results

5.3.1 Pupillograms

Protocol 1 with white led stimulus on the left eye on five different subjects

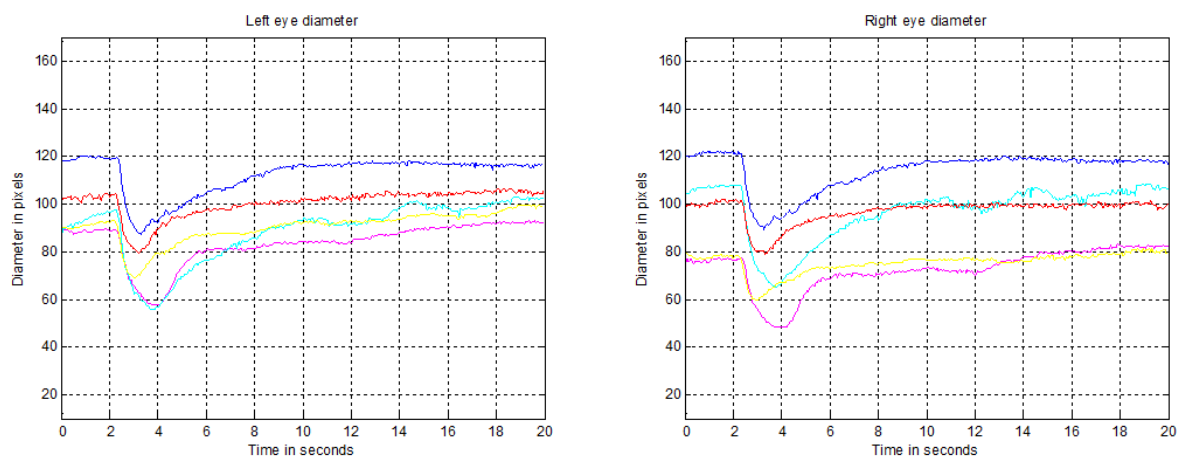


Figure 5. 1 : Pupil response in white led stimulus in the left eye

Protocol 1 with white led stimulus on the right eye on five different subjects

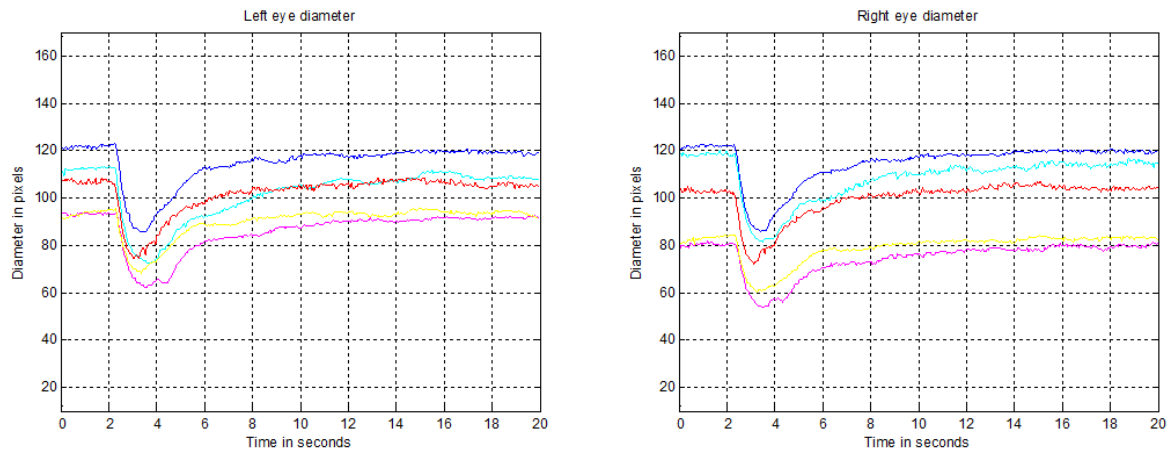


Figure 5. 2: Pupil response in white led stimulus in the right eye

Protocol 2 at the same subject with white led stimulus on the left eye

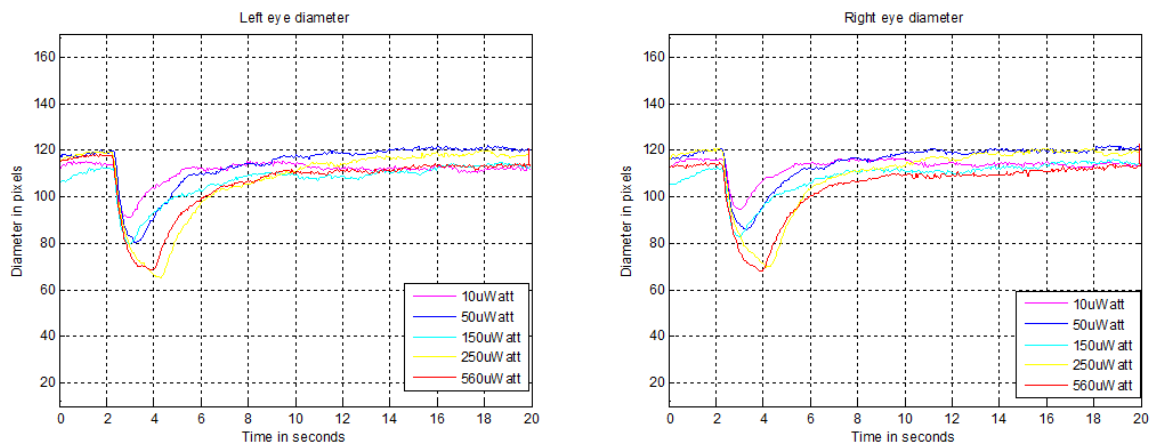


Figure 5. 3: Pupil response in white led stimulus in the left eye with various intensities

Protocol 2 at the same subject with white led stimulus on the right eye

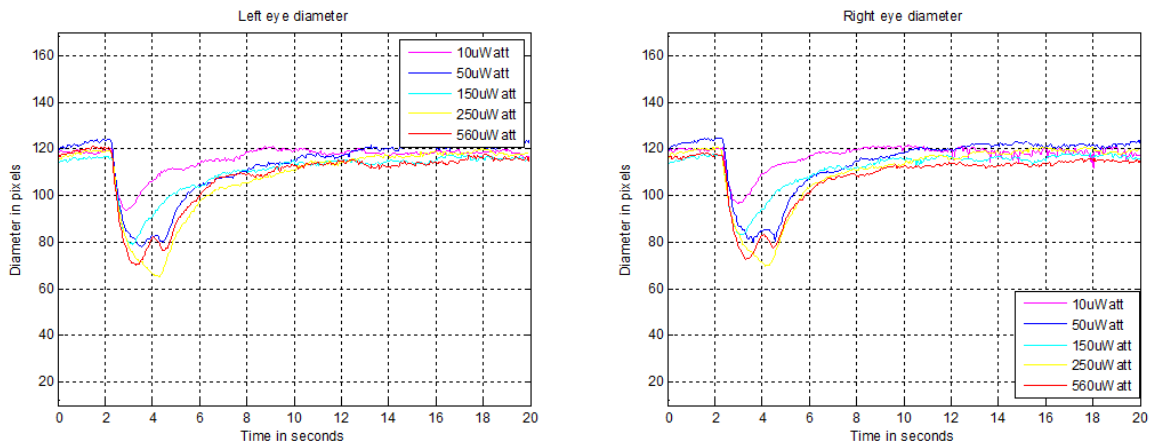


Figure 5. 4: Pupil response in white led stimulus in the right eye with various intensities

Protocol 3 with monochromatic led stimulus on the same subject

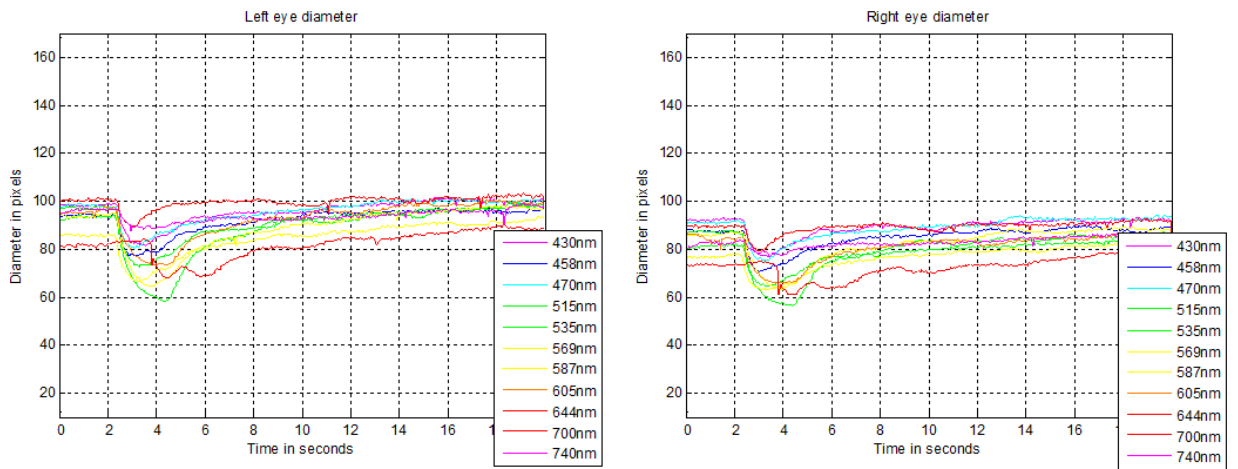


Figure 5. 5: Pupil response with stimulus in the left eye

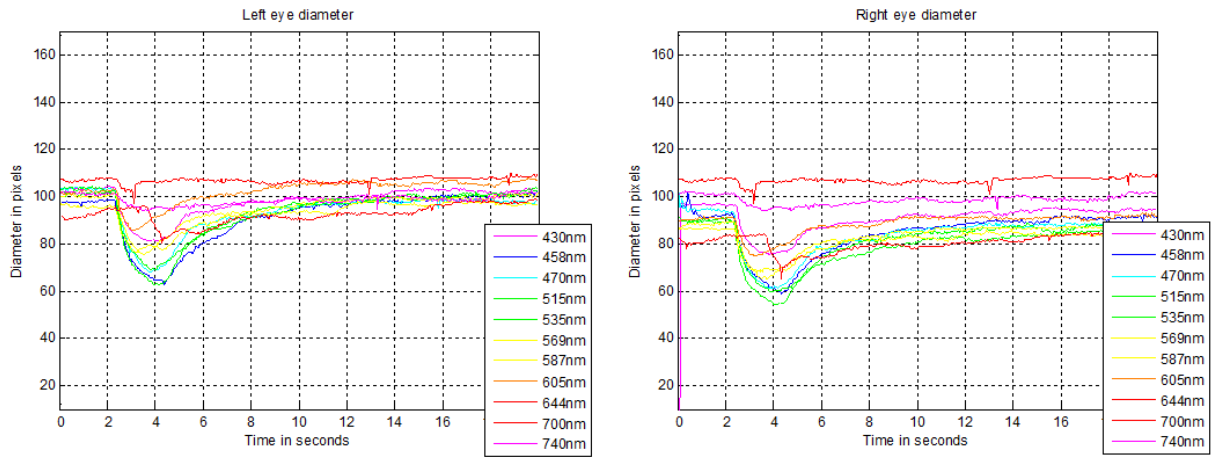


Figure 5. 6: Pupil response with stimulus in the right eye

5.3.2 Parameter analysis

The above diagrams are a characteristic sample of the collected data. The five subjects have a uniform and expected behavior which is shown in the following parameter analysis.

Considering the experimental procedure and the form of a pupillograms, eleven parameters are defined and calculated in the whole sample.

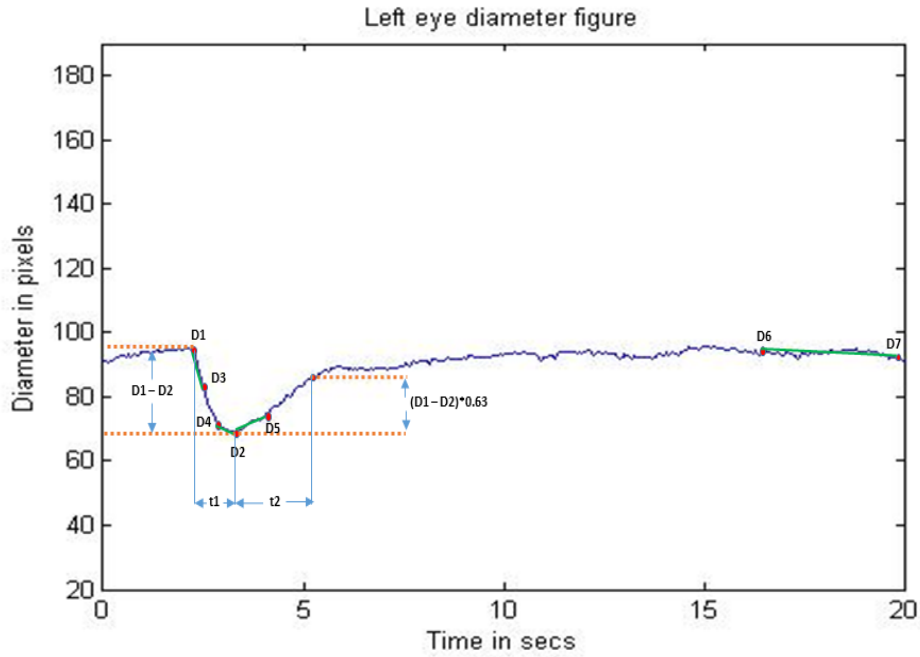


Figure 5. 7: Parameters definition diagram

The parameters of the above diagram are:

- D1: Initial diameter
- D2: Minimum diameter
- Cr: Constriction ratio = $(D1-D2)/D1$
- t1: Time to total constriction
- t2: Recovery time
- S1: Slope between points D1-D3
- S2: Slope between points D2-D4
- S3: Slope between points D2-D5
- S4: Slope between points D7-D6
- D8: Mean value between D6-D7
- RR: Recovery ratio = $(D8-D1)/D8$

Having meticulously observed and noted down the eleven (11) aforementioned parameters, it was inferred that six (6) of them should be further elaborated within this piece of research. More specifically, these parameters, which are presented in a detailed way in the appendix, are the following ones: D1, D2, t1, t2, CR% and RR%.

The Constriction Ratio % is considered to be a variable of great significance. In particular, it related to the parameter that provides information regarding the sensitivity of the eye. In essence, it describes the change of the percentage from the initial diameter to the minimum diameter. Put crudely, it relates to the change from the stage of physical inactivity, before the exposure to the given stimulus, to the stage of miosis due to the influence of the stimulus. By dividing the CR% with the time t1, which refers to the time needed for the transition from D1 to D2, a new parameter appears. This particular parameter is associated with the description of the speed of the phenomenon. Further details with reference to this parameter can be found in the appendix.

There are two particular observations, which should be further elaborated. To begin with, emphasis is placed on the results in the case of protocol 2 with various optical power with white led stimulus. The parameter CR%, which describes the sensitivity of the eye regarding the given phenomenon, corroborates a specific theory; an almost linear increase of the sensitivity is expected, when the intensity of the stimulus is following an upward trend, whereas on a later stage saturation and stabilization of the parameter occur. Based on our data, it appears that this change takes place at approximately 250 μ Watt. In the following diagrams, our main objective is twofold; firstly, to include an illustrative description of the deployed theoretical model and, secondly, to present a series of empirical findings, which are seen as the outcomes of the process of data collection.

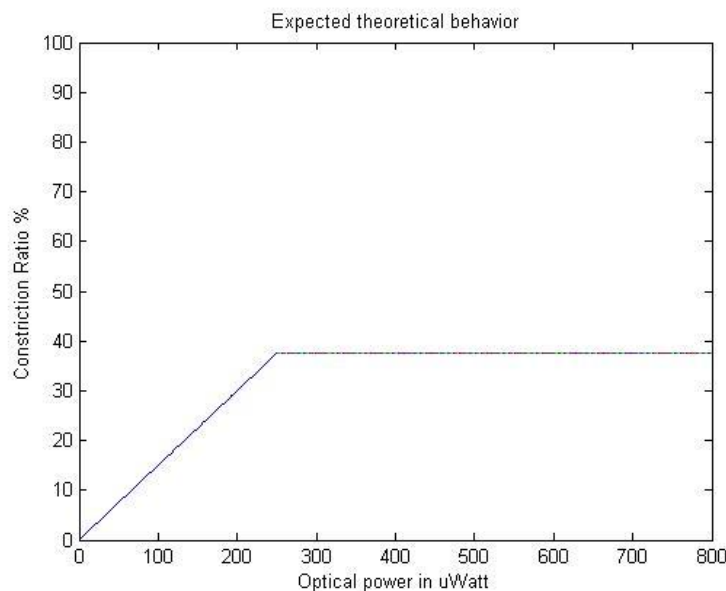


Figure 5. 8: Expected behavior in different intensities

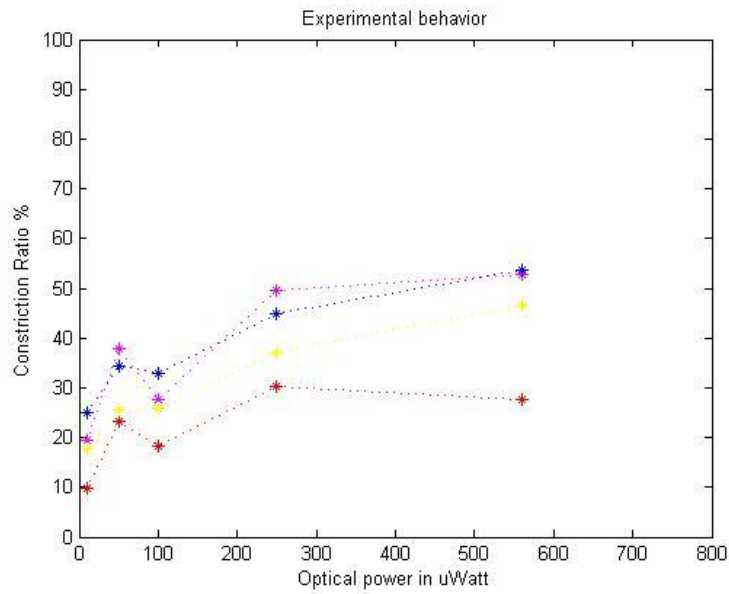


Figure 5.9: Experimental behavior in different intensities

Moving next to the second significant observation, our analysis is focused on the experimental analysis of the monochromatic stimuli. The sensitivity of the optical system in various wavelengths is depicted through the graph of the Gaussian function (bell-shaped curve), which is presented on the following section. By associating the parameter CR% with the sensitivity of the eye, our findings are expected to follow the aforementioned normal distribution. However, it should be noted that the potential existence of outliers in our values are inevitable due to the variability of some of the parameters related to the pupil. During the overall experimental process, precautionary measures were taken, so as to control for the influence of the aforementioned confounding factors. In some cases, these factors could not be fully eliminated.

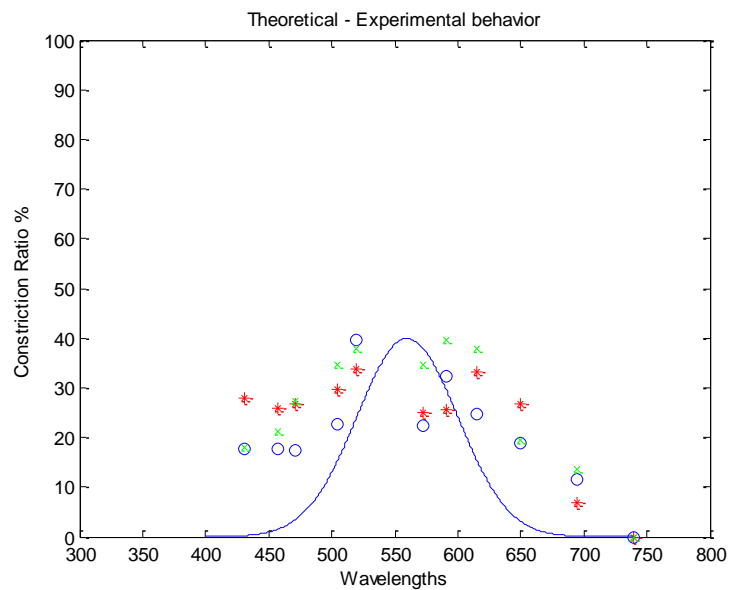


Figure 5.10: Theoretical and experiment behavior in different wavelengths

Furthermore, both of these parameters, namely t_2 and RR%, which relate to the stabilization of the phenomenon, do present an interesting distribution. The process of stabilization after mydriasis is controlled by the parasympathetic autonomous nervous system, whereas miosis is controlled by the sympathetic autonomous nervous system

5.3.3 A different Subject

Apart from the defined as normal group (the five subjects), there is another subject with peculiar behavior. This subject has repeated two times the third protocol. Some pupillograms are presented.

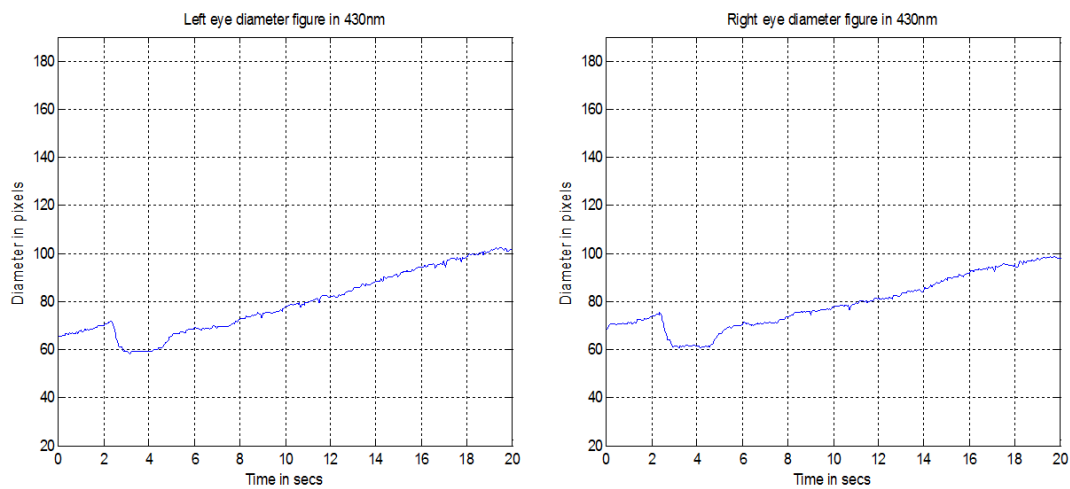


Figure 5. 11: Stimulus in the left eye in 430nm- First measurement

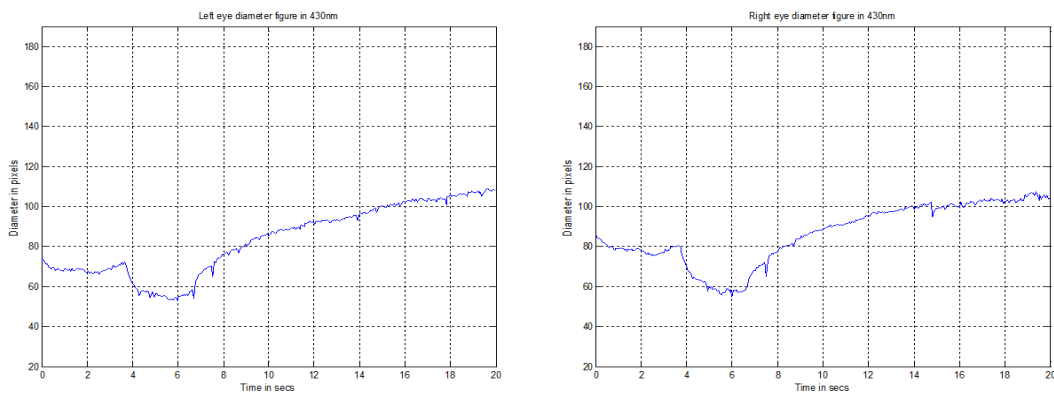


Figure 5. 12: Stimulus in the left eye in 430nm- Second measurement

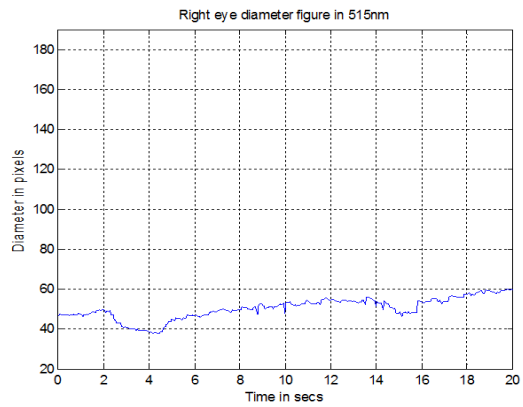
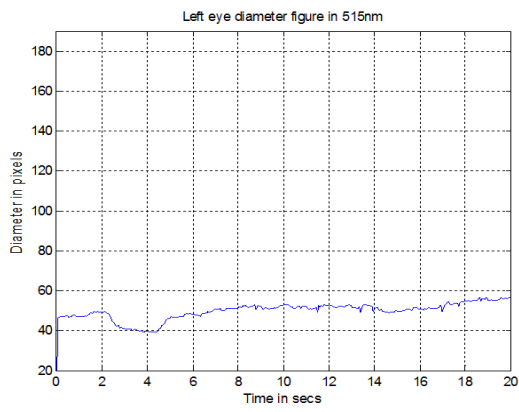


Figure 5. 13: Stimulus in the left eye in 515nm- First measurement

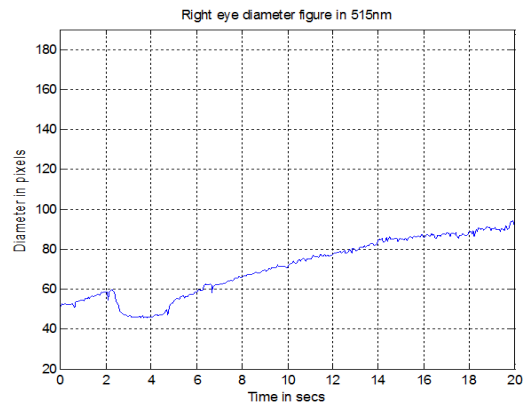
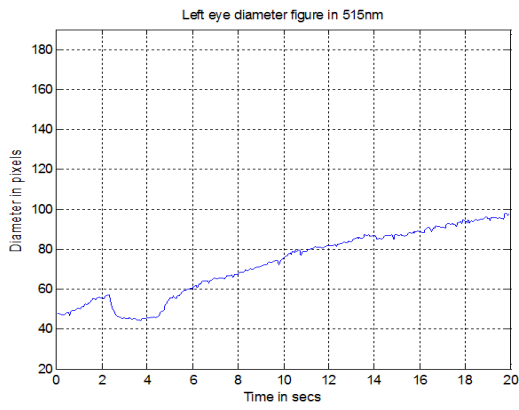


Figure 5. 14: Stimulus in the right eye in 515nm- First measurement

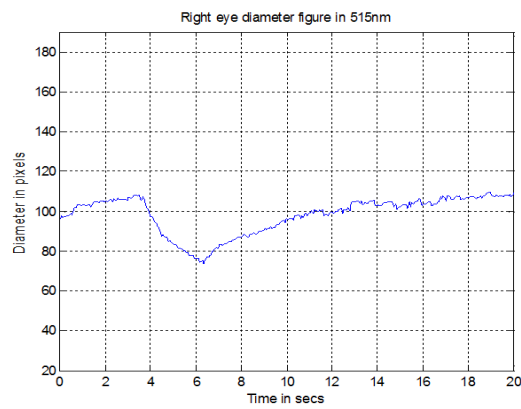
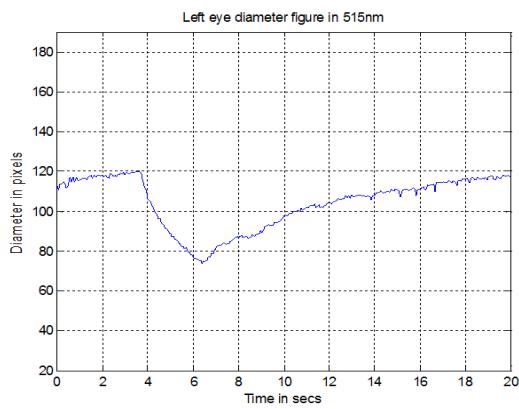


Figure 5. 15: Stimulus in the left eye in 515nm- Second measurement

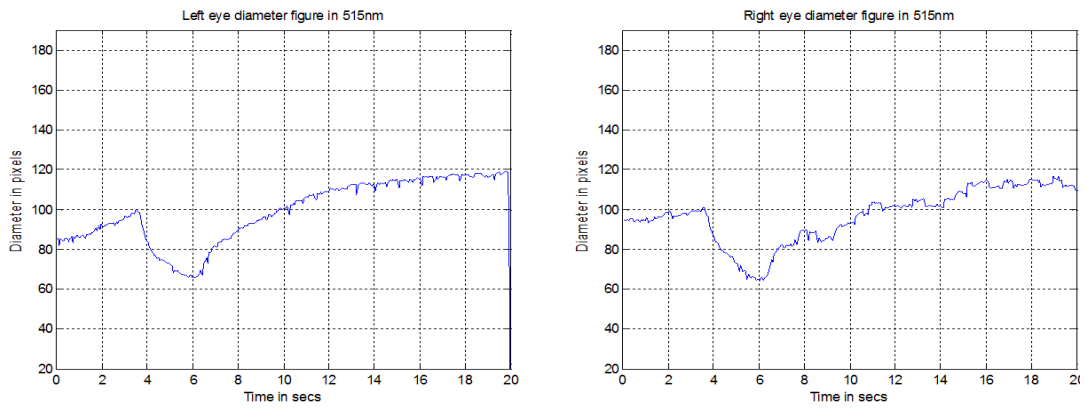


Figure 5. 16: Stimulus in the right eye in 515nm- Second measurement

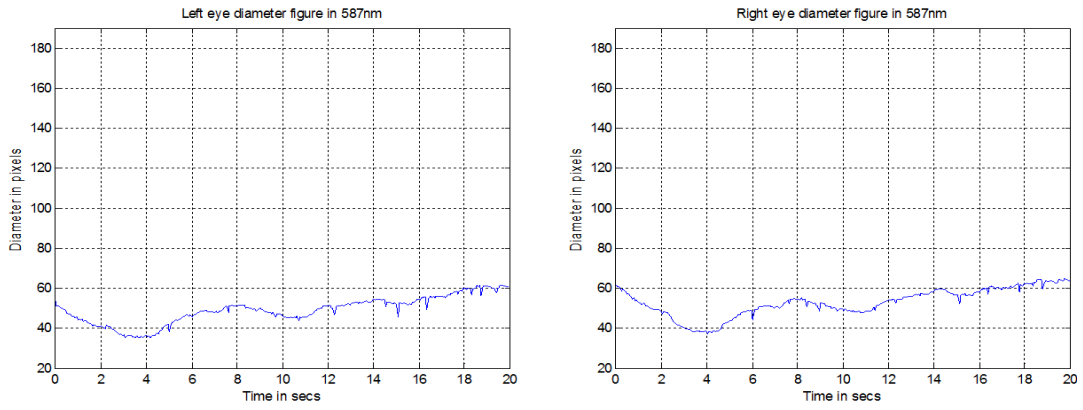


Figure 5. 17: Stimulus in the left eye in 587nm- First measurement

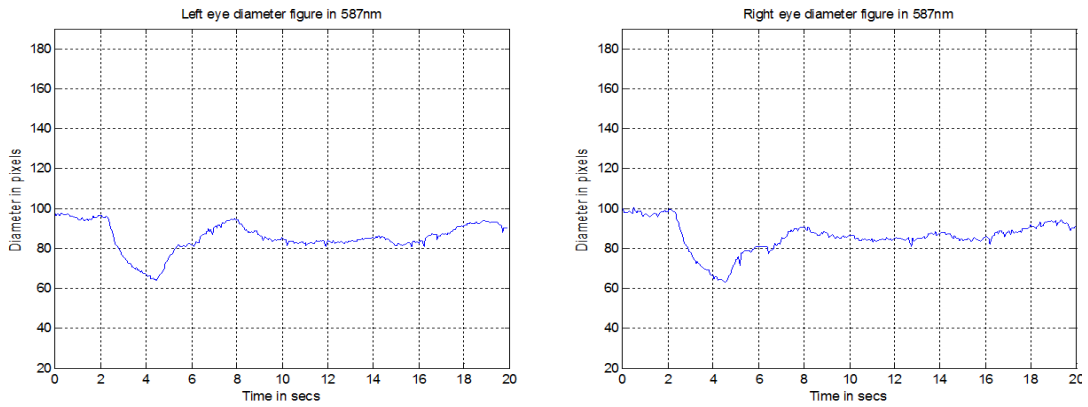


Figure 5. 18: Stimulus in the right eye in 587nm- First measurement

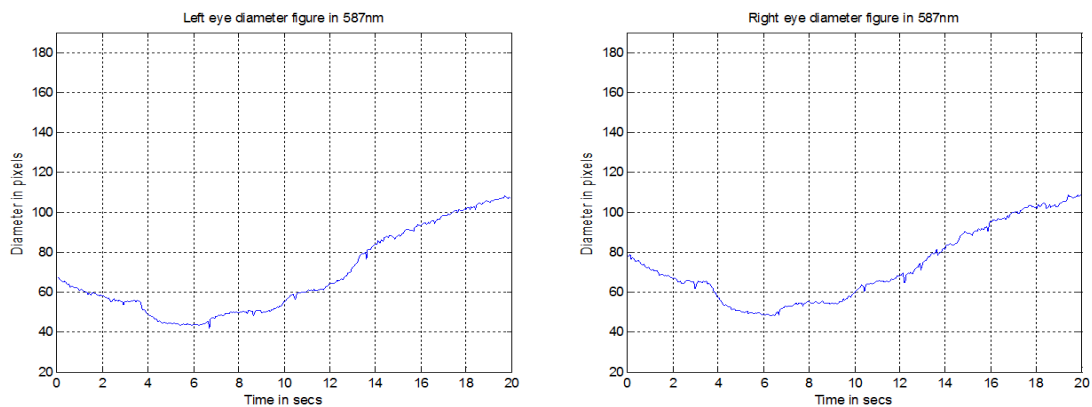


Figure 5. 19: Stimulus in the left eye in 587nm- Second measurement

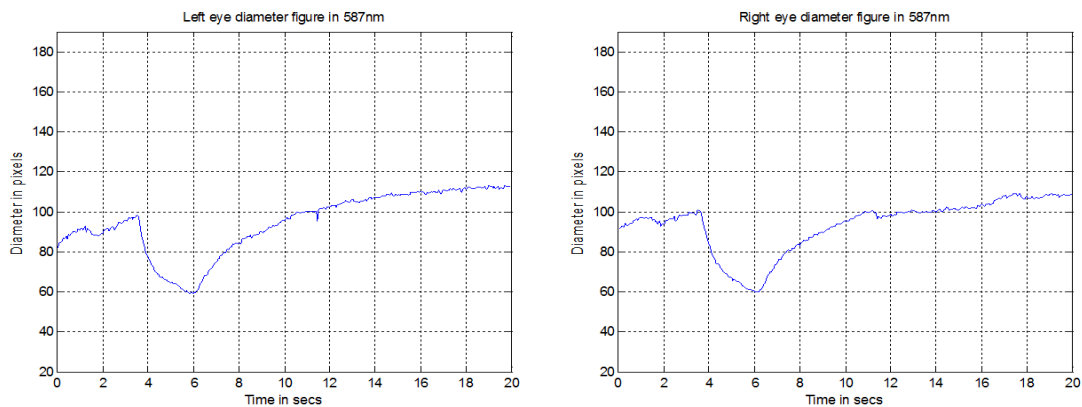


Figure 5. 20: Stimulus in the right eye in 587nm- Second measurement

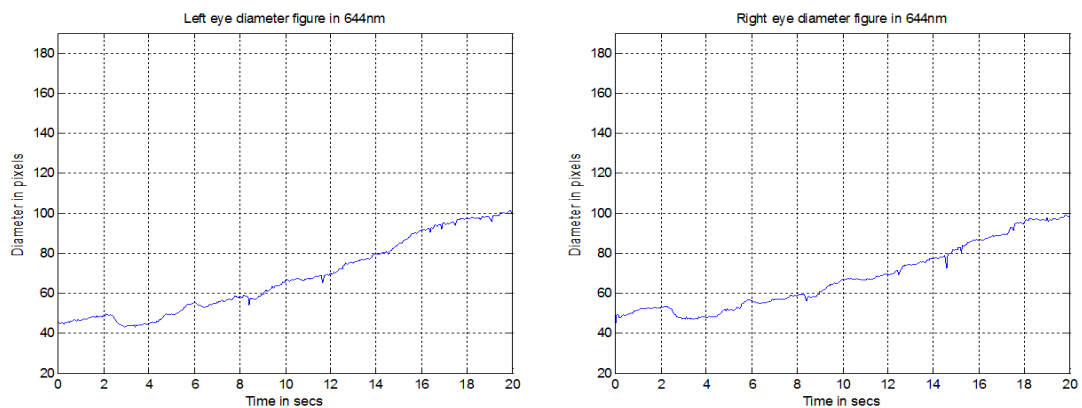


Figure 5. 21: Stimulus in the left eye in 644nm- First measurement

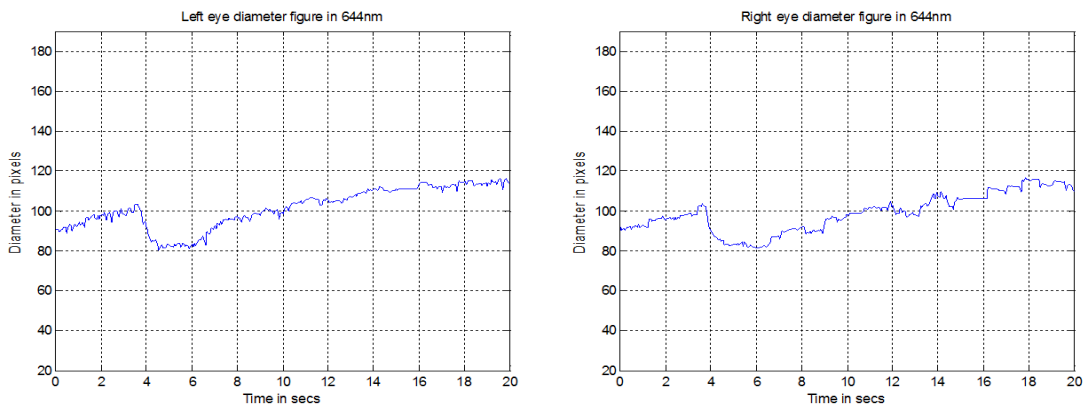


Figure 5. 22: Stimulus in the left eye in 644nm- Second measurement

The first measurement presents an unpredictable behavior and runs counter to the five previous subject's pupillograms. The second measurement approaches better the expected values. In 587nm and with a stimulus in the left eye, the pupillograms present a different behavior in both measurements. This observation it will be a subject for further study in the future, in the specific participant.

5.4 Discussion and Future Work

The empirical study on the aforementioned parameters developed a series of satisfactory inferences. More specifically, the reaction of the pupil is a feature, mainly characterized by its unexpected nature and its significant variances on each occasion. However, there appears to be a stabilization of the parameter, described by the term 'sensitivity', and despite the wide range of the cases, an association between our findings and our expectations is apparent. Besides this, this parameter seems to comply with the theoretical biological estimations.

After having formulated some solid experimental foundations for the aforementioned procedure, the next stages of the current research project will involve data analysis on larger and more socio-demographically diverse population samples. Besides this, after having normalized to a certain extent the samples without a diagnosed pathology, it is proposed that this study will broaden its research focus on clinical cases of a particular diagnosed pathology. In the latter cases, it is expected that the retroreflective feature of the eye will respond differently.

Nevertheless, pupillometry is seen as a largely promising non-intrusive method of timely diagnosis of a wide variety of pathologies and of psychosomatic cases. The use of a pupillometry examination in the field of medicine is considered to be easily undertaken; a speedy and cost-effective procedure, which can provide the examinee with a quantitatively solid bulk of information (instead of a subjective estimation). Given the broad scientific support for this method, its implementation based on targeted and effective clinical trials should be promoted. Thus, it will be

feasible for pupillography to be integrated into the body of approved and efficient clinical methods of examination.

References

- [1] Francesca Regen, Hans Dorn, Heidi Danker-Hopfe
“Association between pupillary unrest index and waking electroencephalogram activity in sleep-deprived healthy adults”
Sleep Medicine 14 (2013) 902–912
- [2] Michael S. Urschitz, Katrin Heine, Lea Mendler, Tobias Peters, Barbara Wilhelm, Christian F. Poets
“Pilot study on the validity of the pupillographic sleepiness test in children and adolescents”
Sleep Medicine 2014 Jun
- [3] Peter L. Franzen, Daniel J. Buysse, Ronald E. Dahl, Wesley Thompson, Greg J. Siegle
“Sleep deprivation alters pupillary reactivity to emotional stimuli in healthy young adults”
Biol Psychol. 2009 March
- [4] A. Merzouki, J. Molero Mesa, A. Louktibi, M. Kadiri, G.V. Urbano
"Assessing changes in pupillary size in Rifian smokers of kif (Cannabis sativa L.)"
Journal of Forensic and Legal Medicine 15, pp. 335–338, 2008
- [5] Edward C. Senay, J.Fred E. Shick
“Pupillometry response to methadone challenge: Aid to diagnosis of opioid dependence”
Drug Alcohol Depend. 1978 Mar;3(2):133-8
- [6] M.A. Phillips · P. Bitsios · E. Szabadi C.M. Bradshaw
“Comparison of the antidepressants reboxetine, fluvoxamine and amitriptyline upon spontaneous pupillary fluctuations in healthy human volunteers”
Psychopharmacology (2000) 149:72–76
- [7] Grünberger J, Linzmayer L, Grunberger M, et al.
“Pupillometry in clinical psychophysiological diagnostics: methodology and proposals for application in psychiatry”
Isr J Psychiatry Relat Sci 1992; 29:100–13
- [8] Adriana L. Bertrand, João Batista Santos Garcia, Erica B. Viera, Alcione M. Santos, and Romero H. Bertrand
“The Influence of Gender and Anxiety on the Pain Response”
European Journal of Pain (Impact Factor: 2.93). 02/2003
- [9] F. Fotiou, K.N. Fountoulakis, M. Tsolaki, A. Goulas, A. Palikaras
"Changes in pupil reaction to light in Alzheimer’s disease patients: a preliminary report"

- International Journal of Psychophysiology 37, pp 111-120, 2000
- [10] Greg J. Siegle, Stuart R. Steinhauer, Michael E. Thase
"Pupillary assessment and computational modeling of the Stroop task in depression"
International Journal of Psychophysiology 52, pp. 63–76, 2004
- [11] Karl-Jürgen Bär, Michael Karl Boettger, Steffen Schulz, Christina Harzendorf, Marcus Willy Agelink, Vikram K. Yeragani, Prtap Chokka, Andreas Voss
"The interaction between pupil function and cardiovascular regulation in patients with acute schizophrenia"
Clin Neurophysiol. 2008 Oct; 119(10):2209-13
- [12] Xiaofei Fan
"Abnormal Transient Pupillary Light Reflex in Individuals with Autism Spectrum Disorders"
J Autism Dev Disord. 2009 November
- [13] Andrew J. Tatham, FRCOphth, Daniel Meira-Freitas, MD, PhD, Robert N. Weinreb, MD, Linda M. Zangwill, PhD, Felipe A. Medeiros, MD, PhD
"Detecting Glaucoma Using Automated Pupillography"
Ophthalmology. 2014 Jun;121 (6):1185-93
- [14] Waisbourd M, Lee B, Ali MH1, Lu L, Martinez P, Faria B, Williams A, Moster MR, Katz LJ, Spaeth GL
"Detection of asymmetric glaucomatous damage using automated pupillography, the swinging flashlight method and the magnified-assisted swinging flashlight method"
Eye (Lond). 2015 Oct;29(10):1321-8
- [15] Annadata V. Rukmini, Dan Milea, Mani Baskaran, Alicia C. Shamira A. Perera, Tin Aung, Joshua J. Gooley
"Pupillary Responses to High-Irradiance Blue Light Correlate with Glaucoma Severity"
Ophthalmology. 2015 Sep;122 (9):1777-85.
- [16] Atsushi Miki, Atsuhiko Iijima, Mineo Takagi, Tomoaki Usui, Shigeru Hasegawa, Haruki Abe, Takehiko Bando
"Pupillography of relative afferent pupillary defect contralateral to monocular mature cataract"
Can J Ophthalmol. 2006 Aug;41(4):469-71
- [17] Matthias Dutsch, Harald Marthol, Georg Michelson, Bernhard Neundorfer, Max Josef Hilz
"Pupillography refines the diagnosis of diabetic autonomic neuropathy"
Journal of the Neurological Sciences 222 (2004) 75– 81
- [18] José Luis Gil Rodríguez, Yaniel Díaz Rubio

“A New Method for Iris Pupil Contour Delimitation and Its Application in Iris Texture Parameter Estimation”

[19] Kavvadias Vasileios

“Imaging System for the pupillary photomotor reflex meter analysis”

Diploma thesis

[20] Rossos Christos

“Development of a computer controlled tunable wavelength light source from ultraviolet to infrared”

Diploma thesis

[21] Balas Kostas

“Human Vision”

Advanced Topics in Electronic Imaging-HPY 603, Graduate Course

Appendix

TABLE KEYS:

ll : stimulus in the left eye and left eye captured

lr : stimulus in the left eye and right eye captured

rr : stimulus in the right eye and left eye captured

rl : stimulus in the right eye and right eye captured

D1	Examinee no1				Examinee no2				Examinee no3				Examinee no4				Examinee no5			
	ll	lr	rl	rr	ll	lr	rl	rr	ll	lr	rl	rr	ll	lr	rl	rr	ll	lr	rl	rr
430nm	115,00	121,40	116,20	123,30	111,00	109,60	113,40	109,30	90,95	78,60	91,49	77,59	99,13	92,07	103,80	96,18	96,38	109,20	93,33	104,10
458nm	116,10	112,40	121,30	117,10	109,70	107,40	112,90	109,10	89,61	76,76	91,82	78,55	93,82	87,89	98,62	92,92	94,09	105,30	92,28	105,80
470nm	113,60	110,80	118,10	118,30	114,10	109,60	115,80	111,20	88,36	79,56	88,62	79,34	97,58	91,25	103,10	93,32	93,59	99,13	108,60	118,70
515nm	113,90	116,00	113,40	116,80	111,20	108,80	116,60	113,90	89,26	77,33	91,26	79,98	93,81	81,66	102,40	89,26	91,04	98,27	99,17	112,10
535nm	108,80	110,70	111,70	117,90	112,00	113,40	114,80	110,70	87,24	75,72	88,78	78,67	96,93	86,54	101,20	90,19	107,60	112,00	110,70	114,70
569nm	115,70	119,20	120,90	119,20	113,00	111,10	109,50	109,30	88,57	73,46	93,83	78,66	85,92	78,10	96,20	86,11	101,20	113,20	108,10	109,70
587nm	116,20	120,90	119,10	123,50	110,50	107,40	115,10	111,60	85,14	77,03	88,14	80,91	95,00	87,43	101,40	89,62	100,20	101,80	86,29	99,81
605nm	115,20	116,30	119,60	119,90	111,40	106,70	113,90	109,40	85,65	74,33	90,78	78,94	97,42	84,75	103,30	91,05	109,40	120,80	93,54	99,55
644nm	105,30	111,40	107,60	117,30	107,60	106,70	113,30	112,20	83,45	72,69	87,90	77,86	83,90	74,10	95,81	84,09	95,92	103,40	91,55	106,20
700nm	112,40	117,80	118,50	125,70	109,40	105,30	112,60	109,30	81,06	73,53	89,66	78,64	100,90	89,63			100,30	108,80	103,80	110,50
740nm																	109,60	116,10	102,60	109,90
white1	119,50	122,10	122,80	121,30	101,80	103,30	105,30	107,90	97,77	92,63	98,91	91,92	94,10	81,30	101,10	87,59	97,75	107,10	110,00	117,80
white2	118,70	120,80	115,80	120,40	104,20	103,90	110,00	106,10	90,08	81,04	96,69	85,62	90,19	72,03	100,00	83,66	99,77	106,80	112,30	118,10
white3	114,50	119,40	119,30	124,90	104,10	103,10	111,30	110,60	95,78	84,89	97,74	85,41	91,34	83,45	101,40	87,92	94,18	102,60	104,40	111,30
white4	108,70	111,70	116,30	116,00	113,80	111,40	116,10	114,60	89,45	77,51	93,28	81,03	92,95	77,98	94,95	84,15	97,24	108,00	112,90	119,00
white5	103,30	114,90	110,80	118,60	103,60	101,70	106,80	102,80	89,27	84,49	91,41	82,22	97,40	82,02	97,57	83,62	98,69	113,60	98,08	116,10
white-10µW	113,80	115,80	119,60	120,80	101,40	105,60	105,80	108,30	83,07	74,67	85,95	78,06	96,69	80,31	108,20	92,94	92,66	106,20	97,02	112,00
white-50µW	119,90	120,60	124,00	124,50	97,15	102,80	103,50	108,10	89,16	78,72	89,09	78,37	112,50	96,83	102,30	89,83	104,00	115,80	93,33	108,30
white-100µW	112,00	112,40	116,50	117,50	101,30	98,48	107,10	104,50	81,04	72,27	83,64	73,63	90,73	83,47	100,80	90,37	97,17	105,20	105,10	111,50
white-250µW	119,10	120,20	119,60	121,20	107,50	108,10	93,02	92,99	89,16	79,08	89,04	77,09	103,70	93,25	100,80	92,95	106,70	112,90	107,10	115,00
white-560µW	117,60	114,30	119,90	116,70	89,98	88,45	87,69	85,55	82,07	71,28	84,13	72,77	96,90	85,00	107,90	94,92	108,00	112,20	98,53	105,70

Table A. 1 Parameter D1

D2	Examinee no1				Examinee no2				Examinee no3				Examinee no4				Examinee no5			
	ll	lr	rl	rr	ll	lr	rl	rr	ll	lr	rl	rr	ll	lr	rl	rr	ll	lr	rl	rr
430nm	66,47	75,54	60,32	70,26	87,28	86,78	81,71	79,16	54,04	44,37	47,22	41,83	81,50	77,30	81,15	75,06	53,28	64,00	52,11	63,20
458nm	64,13	63,45	62,55	63,23	80,79	79,56	83,68	81,43	36,06	31,13	46,07	40,26	77,12	70,41	62,48	59,07	47,49	55,03	50,36	55,64
470nm	78,58	78,67	75,34	76,51	90,43	87,01	84,85	81,82	38,06	34,00	50,05	45,01	80,48	75,06	68,26	61,19	58,22	62,70	65,00	72,44
515nm	67,22	73,21	64,00	67,01	82,84	82,29	82,07	80,11	45,54	40,07	46,96	39,58	72,66	64,30	69,19	59,60	52,81	60,32	65,19	70,17
535nm	73,76	78,23	64,53	70,01	71,97	78,96	76,03	74,96	48,05	43,10	47,29	41,01	58,50	56,52	62,80	54,80	60,32	66,44	57,22	56,84
569nm	93,41	96,72	96,21	95,21	82,64	81,72	82,00	79,61	61,70	51,69	51,01	40,74	66,72	63,07	76,85	68,11	58,59	73,06	68,41	64,74
587nm	92,08	98,20	88,62	94,44	86,41	85,11	85,50	83,68	68,11	61,08	48,41	42,05	64,28	63,07	75,08	65,18	76,94	83,29	58,15	56,50
605nm	96,04	99,61	97,24	94,97	80,36	77,04	76,03	73,02	64,36	55,64	57,22	48,41	73,24	66,00	85,48	74,84	74,64	86,56	63,02	62,49
644nm	90,97	97,26	82,03	92,99	90,75	91,08	83,06	83,64	68,45	60,24	53,22	46,07	68,11	61,01	82,21	70,04	75,57	85,01	59,01	64,45
700nm	99,26	104,90	111,90	118,20	94,68	92,79	104,80	103,10	69,01	61,03	69,23	62,31	89,21	79,29			79,65	86,54	80,83	87,97
740nm																	92,23	100,90	91,52	99,43
white1	87,49	89,44	85,37	89,44	73,16	75,31	70,08	73,10	64,78	59,62	63,73	57,55	70,04	62,04	72,44	62,46	74,00	81,28	75,49	84,24
white2	87,16	88,81	77,40	82,41	80,74	79,61	77,82	79,37	45,28	39,86	60,88	53,11	69,52	56,05	78,24	64,28	74,24	78,22	74,10	78,19
white3	75,44	83,07	76,28	85,05	74,66	74,31	75,44	76,21	63,08	53,95	59,01	51,79	69,34	64,12	80,56	68,42	57,27	66,34	69,78	79,35
white4	63,61	69,76	79,90	82,16	73,62	76,69	77,33	76,73	58,04	48,06	62,03	53,88	69,24	59,60	68,42	61,01	55,52	65,03	72,50	81,50
white5	74,30	81,34	72,47	85,37	80,89	79,16	74,29	71,89	59,65	54,87	52,03	47,01	72,95	62,99	75,34	61,85	67,86	78,85	53,04	63,02
white-10µW	91,17	94,55	93,61	96,31	83,94	86,85	81,17	84,78	61,90	55,10	63,35	58,21	87,31	72,24	93,58	82,00	74,61	85,44	68,70	84,13
white-50µW	80,36	85,68	78,22	79,90	68,25	76,42	69,40	74,00	54,39	47,12	54,31	49,50	86,37	76,00	80,37	70,88	64,47	75,49	59,20	71,06
white-100µW	79,48	82,58	79,09	83,10	75,57	73,04	76,03	77,16	45,30	39,11	53,26	49,65	74,03	68,12	83,49	74,60	70,19	81,34	68,37	74,87
white-250µW	66,18	69,78	79,30	84,17	65,66	68,11	59,44	59,08	42,70	38,00	44,00	40,67	72,44	66,43	65,19	59,05	53,68	58,00	60,21	63,39
white-560µW	68,67	68,01	70,29	72,41	47,37	47,12	46,13	45,30	44,27	36,74	43,00	38,00	70,03	61,07	76,10	67,01	51,11	53,01	44,00	49,01

Table A. 2 Parameter D2

CR%	Examinee no1				Examinee no2				Examinee no3				Examinee no4				Examinee no5			
	ll	lr	rl	rr																
430nm	42,20	37,78	48,09	43,02	21,37	20,82	27,95	27,58	40,58	43,55	48,39	46,09	17,78	16,04	21,82	21,96	44,72	41,39	44,17	39,29
458nm	44,76	43,55	48,43	46,00	26,35	25,92	25,88	25,36	59,76	59,45	49,83	48,75	17,80	19,89	36,65	36,43	49,53	47,74	45,43	47,41
470nm	30,83	29,00	36,21	35,33	20,74	20,61	26,73	26,42	56,93	57,26	43,52	43,27	17,52	17,74	33,79	34,43	37,79	36,75	40,15	38,97
515nm	40,98	36,89	43,56	42,63	25,50	24,37	29,61	29,67	48,98	48,18	48,54	50,51	22,55	21,26	32,43	33,23	41,99	38,62	34,26	37,40
535nm	32,21	29,33	42,23	40,62	35,74	30,37	33,77	32,29	44,92	43,08	46,73	47,87	39,65	34,69	37,94	39,24	43,94	40,68	48,31	50,44
569nm	19,27	18,86	20,42	20,13	26,87	26,44	25,11	27,16	30,34	29,64	45,64	48,21	22,35	19,24	20,11	20,90	42,10	35,46	36,72	40,98
587nm	20,76	18,78	25,59	23,53	21,80	20,75	25,72	25,02	20,00	20,71	45,08	48,03	32,34	27,86	25,96	27,27	23,21	18,18	32,61	43,39
605nm	16,63	14,35	18,70	20,79	27,86	27,80	33,25	33,25	24,86	25,14	36,97	38,67	24,82	22,12	17,25	17,80	31,77	28,34	32,63	37,23
644nm	13,61	12,69	23,76	20,72	15,66	14,64	26,69	25,45	17,97	17,13	39,45	40,83	18,82	17,67	14,19	16,71	21,22	17,79	35,54	39,31
700nm	11,69	10,95	5,57	5,97	13,46	11,88	6,93	5,67	14,87	17,00	22,79	20,77	11,59	11,54			20,59	20,46	22,13	20,39
740nm																	15,85	13,09	10,80	9,53
white1	26,79	26,75	30,48	26,27	28,13	27,10	33,45	32,25	33,74	35,64	35,57	37,39	25,57	23,69	28,35	28,69	24,30	24,11	31,37	28,49
white2	26,57	26,48	33,16	31,55	22,51	23,38	29,25	25,19	49,73	50,81	37,04	37,97	22,92	22,19	21,76	23,17	25,59	26,76	34,02	33,79
white3	34,11	30,43	36,06	31,91	28,28	27,92	32,22	31,09	34,14	36,45	39,63	39,36	24,09	23,16	20,55	22,18	39,19	35,34	33,16	28,71
white4	41,48	37,55	31,30	29,17	35,31	31,16	33,39	33,05	35,11	38,00	33,50	33,51	25,51	23,57	27,94	27,50	42,90	39,79	35,78	31,51
white5	28,07	29,21	34,59	28,02	21,92	22,16	30,44	30,07	33,18	35,06	43,08	42,82	25,10	23,20	22,78	26,03	31,24	30,59	45,92	45,72
white-10µW	19,89	18,35	21,73	20,27	17,22	17,76	23,28	21,72	25,48	26,21	26,29	25,43	9,70	10,05	13,51	11,77	19,48	19,55	29,19	24,88
white-50µW	32,98	28,96	36,92	35,82	29,75	25,66	32,95	31,54	39,00	40,14	39,04	36,84	23,23	21,51	21,44	21,10	38,01	34,81	36,57	34,39
white-100µW	29,04	26,53	32,11	29,28	25,40	25,83	29,01	26,16	44,10	45,88	36,32	32,57	18,41	18,39	17,17	17,45	27,77	22,68	34,95	32,85
white-250µW	44,43	41,95	33,70	30,55	38,92	36,99	36,10	36,47	52,11	51,95	50,58	47,24	30,14	28,76	35,33	36,47	49,69	48,63	43,78	44,88
white-560µW	41,61	40,50	41,38	37,95	47,35	46,73	47,39	47,05	46,06	48,46	48,89	47,78	27,73	28,15	29,47	29,40	52,68	52,75	55,34	53,63

Table A. 3 Parameter CR%

RR%	Examinee no1				Examinee no2				Examinee no3				Examinee no4				Examinee no5			
	ll	lr	rl	rr	ll	lr	rl	rr	ll	lr	rl	rr	ll	lr	rl	rr	ll	lr	rl	rr
430nm	-6,98	-3,32	-6,31	-5,57	-1,19	-0,18	-0,89	4,00	-2,20	0,06	-4,82	-4,95	1,36	0,48	-1,76	-1,64	0,20	-0,92	3,33	2,16
458nm	-0,87	-0,45	-2,71	-2,90	-1,57	-1,13	-1,53	-1,11	-6,82	-6,79	-7,59	-7,50	1,49	1,55	1,48	-2,44	-7,99	-6,87	-1,32	-3,62
470nm	-0,89	-0,45	-2,61	-4,14	-1,06	-0,74	-0,96	-0,29	-2,86	-3,84	-2,14	-3,50	2,52	1,18	-5,60	-5,42	4,54	8,38	-7,10	-6,55
515nm	-4,40	-5,26	-2,62	-3,36	0,54	-0,55	-3,19	-1,79	-4,59	-5,73	-6,45	-6,65	4,06	1,95	-1,49	-4,59	2,43	2,02	0,71	2,01
535nm	-2,06	0,00	-2,57	-3,97	-1,82	-5,00	-3,89	-1,28	-4,93	-5,70	-7,05	-4,82	-0,02	-1,11	0,00	-2,16	-9,32	-7,18	-24,16	-16,12
569nm	-1,49	-2,41	-0,50	1,57	-2,17	-4,22	0,73	0,18	3,82	7,48	-4,69	-4,41	5,80	4,90	1,00	-2,88	1,56	-3,00	-2,56	-5,18
587nm	0,00	0,17	0,25	-0,32	-0,73	-1,42	-0,61	-0,36	3,12	3,25	1,94	3,93	1,96	0,86	-2,70	-2,69	-8,50	-2,63	12,27	6,19
605nm	-1,05	-1,13	0,75	1,48	0,09	0,37	-2,80	-0,18	4,71	5,73	-2,21	-4,17	2,68	1,67	2,55	0,84	-2,53	-3,69	8,74	7,31
644nm	4,19	4,54	3,24	2,09	0,19	0,65	-1,34	-1,81	2,15	0,14	-1,49	-1,50	5,02	5,45	2,45	0,08	-1,66	-0,58	1,89	-1,82
700nm	4,10	2,40	0,34	0,87	0,27	1,03	-1,08	-0,28	2,81	-2,68	-0,66	-0,89	1,56	2,04			2,53	-1,21	-1,37	-2,79
740nm																	2,14	-3,11	0,48	3,26
white1	-2,73	-3,39	-2,76	-0,92	0,49	-2,18	-2,23	-5,37	1,71	2,50	-5,37	-7,36	3,55	3,38	-0,80	-4,14	1,48	1,56	1,43	0,25
white2	-5,98	-3,60	-10,92	-6,64	1,70	-0,48	-1,76	0,19	0,69	2,28	-0,70	-1,45	6,35	7,31	2,25	3,19	8,55	4,13	1,14	-1,37
white3	-0,17	-1,19	-0,59	-1,46	-0,97	-0,88	-1,74	-3,46	3,38	3,80	-4,86	-4,49	2,67	0,51	-0,60	-0,56	2,12	-2,29	2,52	-1,37
white4	-2,55	-4,00	-4,30	-1,13	0,00	0,27	-0,43	-2,87	1,71	4,50	-2,17	-1,54	4,91	1,42	-0,66	-0,61	3,63	-3,35	-3,96	-4,20
white5	-0,29	0,95	0,36	-2,07	2,08	-1,82	-1,14	1,25	-0,79	-1,95	5,27	9,11	1,62	0,92	3,40	0,00	6,37	-0,18	5,87	-0,52
white-10µW	-1,88	-1,22	-0,34	-1,00	-0,40	-2,03	0,28	-0,56	-1,03	-0,13	-1,33	-5,46	7,47	6,50	0,82	0,41	4,20	2,84	2,29	-0,63
white-50µW	1,15	0,74	-1,72	-2,38	2,33	-0,98	-2,58	-2,46	-3,69	-5,00	-0,61	-0,35	-0,54	-2,91	5,80	5,73	-5,38	-3,58	8,50	5,58
white-100µW	1,15	2,18	-0,95	-0,26	0,98	-0,36	-2,59	-1,26	-4,26	-4,82	0,40	1,00	4,86	1,81	0,69	-1,79	-6,43	-5,33	3,67	-2,67
white-250µW	-0,59	-1,26	0,25	0,08	-2,97	-4,04	-5,30	-5,12	-9,78	-10,29	-8,22	-12,57	-1,67	-0,99	1,18	-2,87	3,18	-3,39	-10,39	-7,78
white-560µW	-4,07	-0,79	-3,99	-1,39	-6,85	-5,86	-6,23	-3,65	-2,30	-4,29	-1,18	-3,13	7,01	5,41	-1,03	-1,31	-17,83	-19,21	1,76	0,19

Table A. 4 Parameter PR%

t1	Examinee no1				Examinee no2				Examinee no3				Examinee no4				Examinee no5			
	ll	lr	rl	rr																
430nm	2,27	2,29	2,03	1,97	0,92	0,89	1,40	1,33	2,04	1,98	2,16	2,24	1,26	1,03	1,46	1,44	1,44	1,48	1,69	1,57
458nm	2,00	1,92	2,04	2,05	1,14	0,91	0,99	0,85	2,23	2,16	2,03	1,92	0,54	0,72	2,11	2,10	1,81	1,81	2,29	2,28
470nm	1,03	1,10	1,68	1,60	0,84	0,88	2,03	2,14	2,26	2,16	1,91	1,64	0,79	0,92	1,49	1,68	1,10	1,14	1,62	1,69
515nm	1,88	1,73	2,03	2,02	1,02	0,77	1,83	1,75	2,16	2,22	2,16	2,21	1,02	1,03	1,70	1,61	1,28	1,09	2,15	2,16
535nm	0,96	0,99	2,03	1,97	2,16	2,23	2,28	2,10	2,17	2,05	2,22	1,64	2,10	2,24	1,86	2,16	2,14	2,18	1,87	2,10
569nm	0,76	1,03	0,62	0,84	0,92	0,84	0,71	0,72	1,38	1,20	2,06	2,10	1,08	1,08	1,00	2,11	1,80	1,86	1,61	1,67
587nm	0,72	1,09	0,94	0,97	1,06	0,85	0,96	1,00	0,83	0,67	1,59	1,73	1,53	1,65	1,21	1,12	0,95	0,95	1,56	1,87
605nm	0,64	0,65	0,66	0,60	0,90	0,79	1,07	1,07	0,92	1,01	2,07	2,05	2,17	1,85	0,88	0,98	1,31	1,11	2,13	1,99
644nm	0,66	0,44	0,82	0,84	0,85	0,72	1,38	1,20	1,24	1,13	1,67	1,56	0,90	0,85	0,90	0,84	0,77	0,72	2,15	2,16
700nm	0,66	0,46	0,54	0,48	0,40	0,66	0,59	0,41	1,57	1,91	1,98	1,91	0,66	0,62			0,79	0,76	1,77	1,50
740nm																	1,55	1,03	0,78	0,83
white1	1,02	1,10	1,19	0,94	0,84	0,89	1,50	1,33	2,24	2,35	2,28	2,22	1,09	1,02	1,61	1,68	0,89	0,89	0,90	0,89
white2	1,14	1,26	1,30	1,60	0,95	0,90	1,32	1,39	2,11	2,19	2,40	2,33	0,84	0,91	1,38	0,97	1,06	0,88	1,48	1,63
white3	1,70	1,51	1,98	1,92	0,85	0,78	1,33	1,26	2,31	2,22	2,30	2,16	1,87	1,02	0,84	0,80	1,38	1,62	1,07	1,32
white4	1,98	2,16	0,90	0,91	2,22	1,14	1,14	1,02	1,79	1,57	1,27	1,27	0,84	0,75	1,20	1,20	1,56	1,50	1,50	1,21
white5	0,97	0,85	1,06	0,96	1,04	1,05	1,24	1,03	1,36	1,26	2,04	2,16	0,83	0,90	1,15	1,26	1,51	1,56	2,06	2,21
white-10μW	0,67	0,66	0,61	0,65	0,48	0,53	0,70	0,88	1,02	1,09	1,09	1,14	0,59	0,72	1,11	0,76	0,85	0,66	0,90	0,79
white-50μW	0,98	1,03	1,37	1,32	0,66	0,61	0,55	1,32	2,46	2,51	1,98	1,67	1,29	1,44	0,99	1,04	1,21	1,14	0,92	1,05
white-100μW	0,72	0,79	0,89	0,84	0,80	0,67	1,48	1,42	1,96	1,92	2,69	2,59	0,80	0,85	0,74	0,88	1,39	1,27	1,19	0,96
white-250μW	2,18	1,97	0,96	0,96	2,23	2,09	1,73	1,87	2,46	2,24	2,51	2,55	1,83	1,85	2,14	2,36	1,63	1,54	1,84	1,78
white-560μW	1,61	1,75	1,11	1,01	2,10	1,80	2,25	2,16	1,68	1,59	2,14	2,28	0,96	1,05	1,41	1,37	1,75	2,24	2,03	2,27

Table A. 5 Parameter t1

t2	Examinee no1				Examinee no2				Examinee no3				Examinee no4				Examinee no5			
	ll	lr	rl	rr																
430nm	1,92	1,75	2,10	2,05	1,79	1,68	1,96	2,40	1,44	1,38	2,72	2,39	1,81	1,92	3,21	2,88	3,74	3,60	2,50	2,63
458nm	2,59	2,17	2,61	2,57	2,46	2,68	2,34	2,22	2,70	2,40	2,57	2,69	2,77	2,70	2,64	2,83	2,92	3,06	2,17	2,40
470nm	2,75	2,61	1,81	2,11	2,01	2,32	2,05	1,85	2,99	3,48	2,21	2,71	2,60	2,31	3,00	3,41	3,10	2,83	4,84	4,66
515nm	3,16	2,94	2,55	1,93	2,16	2,23	1,91	2,03	2,35	2,40	2,04	2,46	2,34	2,33	3,60	4,56	3,12	2,44	2,40	2,78
535nm	4,25	3,25	3,47	2,71	1,57	1,50	1,86	1,80	1,98	2,16	3,05	4,49	2,05	1,90	2,16	2,24	2,52	2,45	6,05	5,17
569nm	3,43	2,99	1,41	1,20	2,33	2,35	2,16	2,05	1,86	2,40	2,75	2,82	2,46	2,34	2,67	2,34	2,22	2,32	3,53	3,23
587nm	2,92	2,05	2,41	2,33	1,88	2,03	2,28	1,92	2,11	2,34	2,20	2,44	2,85	2,19	2,45	2,51	2,34	1,86	1,20	1,79
605nm	1,28	1,20	1,81	1,92	1,80	1,75	2,53	2,71	1,35	1,31	2,16	2,16	2,63	2,23	1,78	1,96	2,12	2,31	2,08	2,09
644nm	2,28	2,34	2,33	2,09	2,01	1,99	1,31	1,80	1,68	1,78	2,65	3,17	3,31	3,00	7,02	3,36	4,08	4,26	2,29	2,34
700nm	1,44	1,93	0,79	1,02	1,31	1,00	0,97	0,97	1,55	3,85	1,50	1,90	1,16	1,06			4,73	5,04	1,80	1,97
740nm																	2,40	2,98	3,19	1,38
white1	3,85	3,98	2,05	3,64	1,75	1,92	1,68	1,69	1,33	1,60	1,38	1,26	2,40	2,93	2,53	3,20	2,36	2,40	3,63	3,49
white2	2,88	3,05	3,91	1,99	1,79	2,28	1,73	1,62	2,21	2,12	1,56	1,51	1,67	1,38	2,47	2,57	1,40	1,62	2,39	2,15
white3	2,16	1,73	2,34	2,10	1,85	1,70	2,57	2,27	1,60	1,60	1,12	1,02	2,10	3,46	2,16	2,50	2,75	2,76	2,29	2,11
white4	3,23	2,88	2,70	2,45	1,75	2,69	2,46	2,52	1,38	1,37	2,53	2,70	1,98	1,88	1,80	1,98	3,12	3,12	3,87	3,90
white5	2,24	2,27	2,37	2,71	1,50	2,03	1,76	1,87	1,82	1,92	1,56	1,44	3,75	3,57	2,34	4,80	1,62	1,93	1,78	1,99
white-10μW	1,38	1,14	1,55	1,38	1,06	1,68	1,56	1,38	2,16	1,98	2,02	2,00	1,68	0,89	2,88	2,60	2,34	2,69	2,80	2,88
white-50μW	1,77	1,81	3,16	2,52	1,93	1,98	2,98	2,03	2,20	2,11	1,48	1,44	2,64	3,60	2,66	2,08	3,75	3,18	2,26	2,42
white-100μW	2,09	1,78	2,05	2,05	1,49	1,79	2,05	1,87	2,26	2,23	1,58	1,49	2,19	2,33	2,14	2,72	3,36	3,63	2,99	3,65
white-250μW	1,92	1,68	2,27	2,34	2,39	2,42	1,52	1,32	1,87	2,02	2,28	2,31	2,97	2,29	2,94	2,22	2,79	3,01	2,63	2,63
white-560μW	2,23	1,68	2,81	2,53	1,54	1,63	1,17	1,36	2,53	2,82	3,28	3,37	2,46	2,02	3,44	2,88	3,99	3,53	2,58	2,42

Table A. 6 Parameter t2

CR%/t1	Examinee no1				Examinee no2				Examinee no3				Examinee no4				Examinee no5			
	ll	lr	rl	rr																
430nm	18,59	16,50	23,69	21,84	23,23	23,39	19,96	20,73	19,89	21,99	22,40	20,58	14,11	15,57	14,95	15,25	31,05	27,97	26,13	25,02
458nm	22,38	22,68	23,74	22,44	23,12	28,49	26,14	29,84	26,80	27,52	24,54	25,39	32,96	27,62	17,37	17,35	27,36	26,38	19,84	20,79
470nm	29,93	26,36	21,55	22,08	24,70	23,42	13,17	12,35	25,19	26,51	22,79	26,38	22,18	19,29	22,68	20,49	34,36	32,24	24,78	23,06
515nm	21,80	21,32	21,46	21,10	25,00	31,64	16,18	16,95	22,68	21,70	22,47	22,86	22,10	20,64	19,08	20,64	32,81	35,43	15,94	17,32
535nm	33,55	29,63	20,80	20,62	16,55	13,62	14,81	15,37	20,70	21,01	21,05	29,19	18,88	15,49	20,40	18,17	20,53	18,66	25,83	24,02
569nm	25,35	18,31	32,94	23,96	29,20	31,48	35,37	37,73	21,98	24,70	22,15	22,96	20,69	17,82	20,11	9,91	23,39	19,06	22,80	24,54
587nm	28,83	17,23	27,23	24,26	20,57	24,42	26,79	25,02	24,10	30,90	28,35	27,76	21,14	16,89	21,45	24,35	24,44	19,14	20,90	23,20
605nm	25,99	22,08	28,33	34,65	30,96	35,19	31,07	31,08	27,02	24,90	17,86	18,87	11,44	11,96	19,60	18,17	24,25	25,54	15,32	18,71
644nm	20,62	28,85	28,98	24,67	18,42	20,33	19,34	21,21	14,50	15,16	23,63	26,17	20,91	20,78	15,77	19,89	27,55	24,70	16,53	18,20
700nm	17,71	23,81	10,31	12,43	33,64	18,00	11,74	13,84	9,47	8,90	11,51	10,87	17,55	18,61			26,06	26,92	12,50	13,59
740nm																	10,22	12,71	13,85	11,48
white1	26,26	24,32	25,61	27,94	33,49	30,44	22,30	24,25	15,06	15,16	15,60	16,84	23,46	23,23	17,61	17,08	27,30	27,09	34,86	32,01
white2	23,31	21,02	25,51	19,72	23,70	25,98	22,16	18,12	23,57	23,20	15,43	16,30	27,28	24,38	15,77	23,88	24,14	30,41	22,98	20,73
white3	20,07	20,15	18,21	16,62	33,27	35,80	24,22	24,68	14,78	16,42	17,23	18,22	12,88	22,71	24,47	27,72	28,40	21,82	30,99	21,75
white4	20,95	17,38	34,78	32,06	15,90	27,33	29,29	32,40	19,62	24,20	26,38	26,38	30,37	31,43	23,28	22,92	27,50	26,52	23,86	26,04
white5	28,94	34,36	32,64	29,19	21,08	21,11	24,55	29,19	24,40	27,82	21,12	19,83	30,24	25,78	19,81	20,66	20,69	19,61	22,29	20,69
white-10μW	29,68	27,80	35,62	31,19	35,87	33,50	33,26	24,68	24,98	24,04	24,12	22,31	16,44	13,96	12,17	15,49	22,92	29,62	32,43	31,50
white-50μW	33,65	28,11	26,95	27,14	45,07	42,07	59,90	23,90	15,85	15,99	19,72	22,06	18,01	14,94	21,65	20,28	31,41	30,54	39,75	32,75
white-100μW	40,33	33,58	36,08	34,85	31,75	38,56	19,60	18,42	22,50	23,90	13,50	12,57	23,01	21,64	23,21	19,83	19,98	17,86	29,37	34,22
white-250μW	20,38	21,29	35,10	31,83	17,45	17,70	20,87	19,50	21,18	23,19	20,15	18,53	16,47	15,55	16,51	15,45	30,49	31,58	23,79	25,21
white-560μW	25,84	23,14	37,28	37,58	22,55	25,96	21,06	21,78	27,42	30,48	22,85	20,96	28,89	26,81	20,90	21,46	30,10	23,55	27,26	23,63

Table A. 7 Parameter CR%/t1

D1	Examinee no6-1rst Meas				Examinee no6-2nd Meas				D2	Examinee no6-1rst Meas				Examinee no6-2nd Meas			
	ll	lr	rl	rr	ll	lr	rl	rr		ll	lr	rl	rr	ll	lr	rl	rr
430nm	68,13	74,60	48,21	51,56	72,27	80,53	72,65	83,1	430nm	55,64	60,49	39,35	43,32	53,09	55,98	59,68	67,36
458nm	93,44	94,95	46,19	54,15	119,30	113,40	109,40	105,2	458nm	62,27	61,69	40,70	46,39	83,01	83,55	86,16	84,40
470nm	59,88	68,42	62,97	73,49	82,48	89,01	116,00	105,1	470nm	44,00	50,07	46,35	52,86	62,04	68,11	84,19	77,39
515nm	47,24	48,57	56,76	58,81	119,50	111,50	100,10	102,9	515nm	37,11	37,57	44,00	44,96	75,37	76,15	65,28	67,95
535nm	55,45	64,74	45,28	52,33	118,80	108,40	117,20	113,5	535nm	39,02	41,65	35,12	38,05	76,62	71,74	72,69	72,89
569nm	63,69	71,61	50,41	58,64	96,12	104,60	100,10	103,2	569nm	48,13	52,41	37,01	41,91	69,00	74,61	65,28	67,15
587nm	41,11	47,71	96,59	98,53	55,95	65,24	98,81	100,4	587nm	36,06	38,08	64,71	63,15	43,49	48,04	59,62	60,17
605nm	55,40	60,53	47,01	49,70	109,50	99,66	118,10	113,8	605nm	46,10	48,16	37,01	38,10	71,78	75,76	73,55	73,53
644nm					102,00	102,90	102,00	103,7	644nm					82,24	82,00	82,24	81,67
700nm					113,60	110,50	107,80	105,7	700nm					99,39	97,42	93,13	93,77
740nm									740nm								
white	62,73	70,35	58,78	68,38	79,56	89,70	65,20	78,01	white	45,11	51,71	46,00	51,99	57,41	64,17	53,01	60,98
CR%	Examinee no6-1rst Meas				Examinee no6-2nd Meas				RR%	Examinee no6-1rst Meas				Examinee no6-2nd Meas			
	ll	lr	rl	rr	ll	lr	rl	rr		ll	lr	rl	rr	ll	lr	rl	rr
430nm	18,33	18,91	18,38	15,98	26,54	30,49	17,85	18,94	430nm	28,50	21,46	50,08	46,82	31,43	22,42	35,19	24,18
458nm	33,36	35,03	11,89	14,33	30,42	26,32	21,24	19,77	458nm	8,93	4,52	54,54	47,38	-3,20	-4,04	9,96	6,16
470nm	26,52	26,82	26,39	28,07	24,78	23,48	27,42	26,37	470nm	34,98	26,18	18,35	12,14	27,97	9,87	1,94	5,49
515nm	21,44	22,65	22,48	23,55	36,93	31,70	34,79	33,97	515nm	8,59	13,48	37,97	32,53	-4,37	-1,64	10,47	10,05
535nm	29,63	35,67	22,44	27,29	35,51	33,82	37,98	35,78	535nm	26,63	13,22	34,57	25,33	-7,41	-3,04	-0,34	1,56
569nm	24,43	26,81	26,58	28,53	28,21	28,67	34,79	34,93	569nm	36,69	29,52	2,02	-6,39	16,20	6,77	10,47	9,39
587nm	12,28	20,18	33,01	35,91	22,27	26,36	39,66	40,07	587nm	31,68	23,10	-4,52	-8,35	44,16	35,91	10,66	6,26
605nm	16,79	20,44	21,27	23,34	34,45	23,98	37,72	35,39	605nm	15,26	10,51	42,79	39,18	3,95	11,33	-2,43	1,81
644nm					19,37	20,31	19,37	21,24	644nm					10,99	8,12	10,05	7,41
700nm					12,51	11,84	13,61	11,29	700nm					5,18	7,76	9,49	7,44
740nm									740nm								
white	28,09	26,50	21,74	23,97	27,84	28,46	18,70	21,83	white	16,28	10,55	-0,72	-5,09	23,50	17,86	40,24	27,84
t1	Examinee no6-1rst Meas				Examinee no6-2nd Meas				t2	Examinee no6-1rst Meas				Examinee no6-2nd Meas			
	ll	lr	rl	rr	ll	lr	rl	rr		ll	lr	rl	rr	ll	lr	rl	rr
430nm	0,94	1,74	0,91	2,10	2,33	1,87	1,14	1,12	430nm	1,81	1,27	1,61	0,41	0,96	1,85	1,07	1,55
458nm	2,51	2,76	1,09	1,49	2,88	2,70	2,47	2,64	458nm	2,83	3,07	1,37	1,15	3,93	2,46	1,85	1,86
470nm	1,85	2,09	1,92	2,35	1,61	1,86	2,34	2,40	470nm	1,50	2,00	1,19	2,64	1,50	4,73	3,03	1,98
515nm	2,16	2,18	1,40	1,69	2,82	2,83	2,63	2,69	515nm	0,60	0,58	1,13	1,13	4,63	4,32	2,08	1,81
535nm	2,14	2,16	1,98	2,24	2,75	2,59	2,64	2,69	535nm	8,21	8,65	1,20	1,97	5,20	5,23	3,76	3,84
569nm	1,08	1,79	1,76	2,15	2,57	2,64	2,63	2,70	569nm	1,80	1,50	1,24	1,27	1,36	2,10	2,08	1,73
587nm	2,04	2,11	2,19	2,26	2,58	2,87	2,58	2,58	587nm	0,38	0,73	1,89	2,67	3,27	3,60	1,83	2,03
605nm	1,02	1,14	2,35	1,97	2,81	2,99	2,67	2,59	605nm	1,68	1,61	0,49	0,61	2,71	1,09	3,18	2,52
644nm					2,27	2,58	2,27	2,52	644nm					1,20	2,76	1,33	2,93
700nm					0,65	0,83	1,01	0,84	700nm					2,53	2,58	2,56	2,88
740nm									740nm								
white	2,16	2,28	1,97	2,17	2,28	2,40	1,48	1,63	white	8,36	8,61	0,72	0,77	2,27	2,75	1,10	1,01
CR%/t1	Examinee no6-1rst Meas				Examinee no6-2nd Meas												
	ll	lr	rl	rr	ll	lr	rl	rr	ll	lr	rl	rr	ll	lr	rl	rr	
430nm	19,50	10,87	20,20	7,61	11,39	16,30	15,66	16,91									
458nm	13,29	12,69	10,90	9,62	10,56	9,75	8,60	7,49									
470nm	14,33	12,83	13,75	11,95	15,39	12,62	11,72	10,99									
515nm	9,93	10,39	16,06	13,94	13,10	11,20	13,23	12,63									
535nm	13,85	16,51	11,33	12,18	12,91	13,06	14,39	13,30									
569nm	22,62	14,98	15,10	13,27	10,98	10,86	13,23	12,94									
587nm	6,02	9,57	15,07	15,89	8,63	9,19	15,37	15,53									
605nm	16,46	17,93	9,05	11,85	12,26	8,02	14,13	13,66									
644nm					8,53	7,87	8,53	8,43									
700nm					19,24	14,26	13,47	13,44									
740nm																	
white	13,00	11,62	11,04	11,05	12,21	11,86	12,63	13,39									

Table A. 8 Parameters for the sixth subject